iScience

CellPress

Article

Ezh2 Controls Skin Tolerance through Distinct Mechanisms in Different Subsets of Skin Dendritic Cells

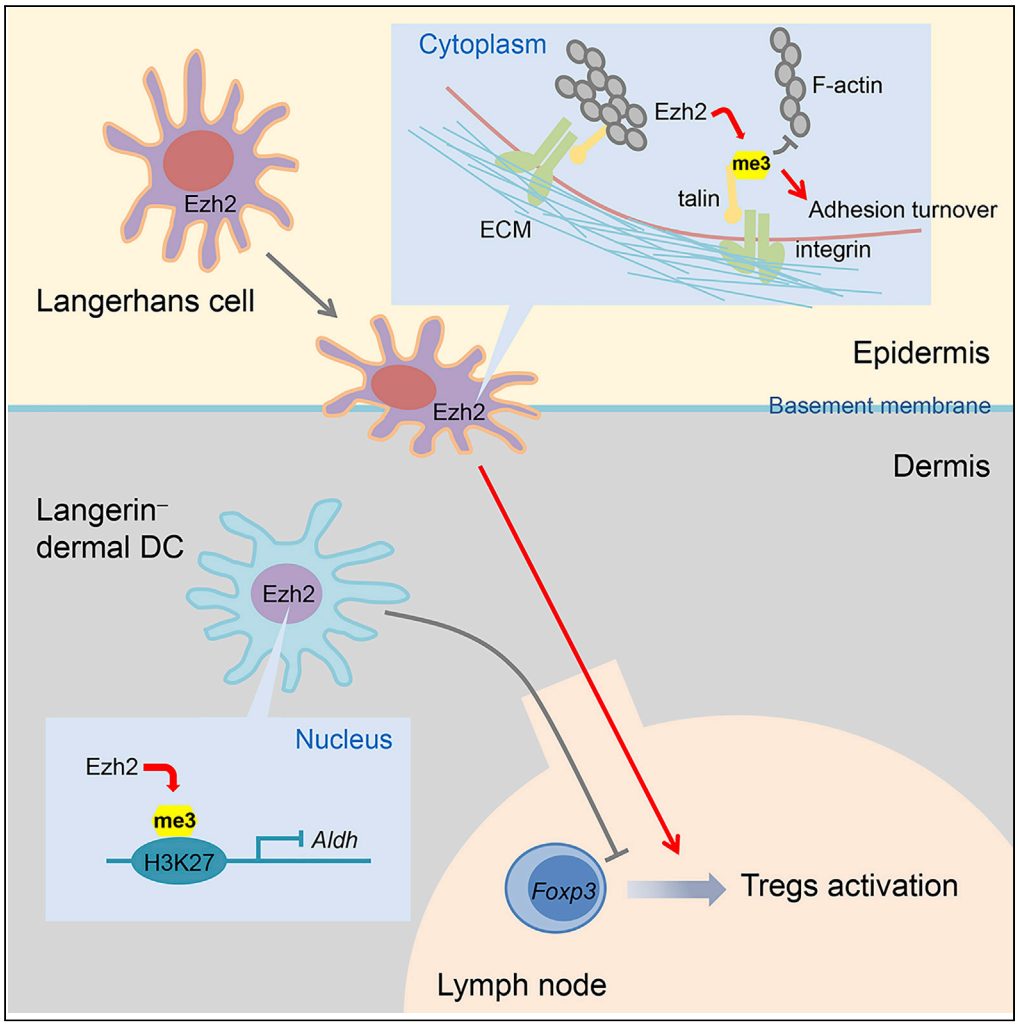

Jia Tong Loh, Thomas Jun Feng Lim, Kyoko Ikumi, ..., Sayuri Yamazaki, Kong-Peng Lam, I-hsin Su

ihsu@ntu.edu.sg

HIGHLIGHTS

Ezh2 regulates LC transmigration across basement membrane via Talin1 methylation

Ezh2-mediated LC migration is required for cutaneous tolerance induction

Ezh2 represses *Aldh* epigenetically in dermal DCs

Ezh2-deficient dermal DCs exhibit increased tolerogenicity

DATA AND SOFTWARE AVAILABILITY

GSE122206

Loh et al., iScience *10*, 23–39
December 21, 2018 © 2018 The Authors.
https://doi.org/10.1016/j.isci.2018.11.019

iScience

CellPress

Article

Ezh2 Controls Skin Tolerance through Distinct Mechanisms in Different Subsets of Skin Dendritic Cells

Jia Tong Loh,[1,2] Thomas Jun Feng Lim,[1] Kyoko Ikumi,[3,4] Takuma Matoba,[3,5] Baptiste Janela,[6] Merry Gunawan,[1] Tatsuya Toyama,[7] Maegan Bunjamin,[1] Lai Guan Ng,[6] Michael Poidinger,[6] Akimichi Morita,[4] Florent Ginhoux,[6] Sayuri Yamazaki,[3] Kong-Peng Lam,[2] and I-hsin Su[1,8,*]

SUMMARY

Ezh2, a well-established epigenetic repressor, can down-regulate leukocyte inflammatory responses, but its role in cutaneous health remains elusive. Here we demonstrate that Ezh2 controls cutaneous tolerance by regulating Langerhans cell (LC) transmigration across the epidermal basement membrane directly via Talin1 methylation. Ezh2 deficiency impaired disassembly of adhesion structures in LCs, leading to their defective integrin-dependent emigration from the epidermis and failure in tolerance induction. Moreover, mobilization of Ezh2-deficient Langerin$^-$ dermal dendritic cells (dDCs) via high-dose treatment with a weak allergen restored tolerance, which is associated with an increased tolerogenic potential of Langerin$^-$ dDCs likely due to epigenetic de-repression of *Aldh* in the absence of Ezh2. Our data reveal novel roles for Ezh2 in governing LC- and dDC-mediated host protection against cutaneous allergen via distinct mechanisms.

INTRODUCTION

The skin is a complex organ that forms the primary barrier against the external environment. Keratinocytes, together with a diverse range of specialized immune cells, form a skin-associated lymphoid tissue that is critical for cutaneous immunosurveillance and host protection against repeated physical and pathogenic insults. Dysregulation of the skin immunity frequently results in various skin pathologies such as allergic contact dermatitis and psoriasis (Kaplan et al., 2005; Stratis et al., 2006).

Langerhans cells (LCs) are a group of professional antigen-presenting dendritic cells (DCs) that strategically populate the epidermis and actively survey the cornified layer for antigens via the extension and retraction of their dendrites (Merad et al., 2002). Despite considerable progress in our understanding of LC biology with the development of various LC ablation and transgenic mouse models, their role in the regulation of skin immunity remains controversial. LC migration to the skin-draining lymph nodes (sdLNs) is required not only for the initiation of adaptive immune responses (Igyarto et al., 2011) but also for the immune suppression during inflammation (Igyarto et al., 2009; Kaplan et al., 2005) and maintenance of steady-state tolerance to innocuous cutaneous antigens and commensal flora (Gomez de Aguero et al., 2012; van der Aar et al., 2013). Yet at the same time they have been demonstrated to be redundant to dermal DCs (dDCs) during skin immunization in different animal models (Fukunaga et al., 2008; Kissenpfennig et al., 2005). Such capacity of LCs to control the balance between immunogenicity and tolerance depends on multiple layers of gene regulation that permit dynamic changes in cellular functions including phagocytosis, migration, and cytokine production (Hacker et al., 2003; Sere et al., 2012). The most extensively studied of these LC regulatory mechanisms is transcriptional control of gene expression, which can potently modulate LC-induced immune responses (Medzhitov and Horng, 2009), but other factors influencing LC-mediated protection against skin injury and inflammation remain only poorly defined.

It is now well-established that leukocyte gene expression can be modified by epigenetic regulatory proteins including enhancer of Zeste homolog 2 (Ezh2), which represses gene expression by catalyzing the addition of methyl groups to histone 3 at lysine 27 (H3K27) (Cao et al., 2002; Czermin et al., 2002). Chromatin remodeling via histone modifications exerts major effects on leukocyte gene expression patterns (Jin et al., 2016; LaMere et al., 2016), but the ability of proteins such as Ezh2 to further modify immune cell function via non-epigenetic mechanisms is less well understood. Given its well-defined role as a

[1]School of Biological Sciences, College of Science, Nanyang Technological University, 60 Nanyang Drive, Singapore 637551, Republic of Singapore

[2]Bioprocessing Technology Institute, Agency for Science, Technology and Research, 20 Biopolis Way, Singapore 138668, Republic of Singapore

[3]Department of Immunology, Nagoya City University Graduate School of Medical Sciences, Nagoya 467-8601, Japan

[4]Department of Geriatric and Environmental Dermatology, Nagoya City University Graduate School of Medical Sciences, Nagoya 467-8601, Japan

[5]Department of Otorhinolaryngology and Head and Neck Surgery, Nagoya City University Graduate School of Medical Sciences, Nagoya 467-8601, Japan

[6]Singapore Immunology Network, Agency for Science, Technology and Research, 8A Biomedical Grove, Singapore 138648, Republic of Singapore

[7]Department of Breast Surgery, Nagoya City University Graduate School of Medical Sciences, Nagoya 467-8601, Japan

[8]Lead Contact

*Correspondence: ihsu@ntu.edu.sg

https://doi.org/10.1016/j.isci.2018.11.019

This is an open access article under the CC BY-NC-ND license (http://creativecommons.org/licenses/by-nc-nd/4.0/).

transcriptional silencer, Ezh2 has previously been implicated in the epigenetic regulation of many immune genes including those associated with host cell defense such as interleukin (IL)-4 and IL-13 (Koyanagi et al., 2005). However, we recently reported an unexpected role for Ezh2 in the post-translational methylation of Talin1, which disrupts Talin1 binding to F-actin and thereby regulates dynamic changes in DC adhesion and migration programs upon encounter with integrin ligands (Gunawan et al., 2015; Loh and Su, 2016).

As Ezh2 has been implicated in the regulation of various immune cell functions including DCs (Gunawan et al., 2015; Su et al., 2003, 2005), and its expression is frequently reduced in patients with cutaneous allergies (De Benedetto et al., 2011), we hypothesized that Ezh2 plays a major role in the control of skin dendritic-cell-mediated protection against skin inflammation. Here we report that Ezh2 critically regulates LC transmigration across the basement membrane via a non-epigenetic mechanism that is essential for the activation of regulatory T cells (Tregs) and host protection against hapten-induced contact hypersensitivity (CHS). Moreover, we identify a subset of skin-resident Ezh2-deficient Langerin$^-$ dDCs with enhanced aldehyde dehydrogenase (ALDH) activity, which can substitute for LCs during tolerance induction via high-dose treatment with a weak hapten. The increased tolerogenicity of Langerin$^-$ dDCs was likely due to epigenetic de-repression of *Aldh* in the absence of Ezh2. Collectively, our data reveal novel roles for Ezh2 in governing LC-migration- and DC-tolerogenicity-mediated host protection against cutaneous allergy.

RESULTS

Ezh2 Controls LC-Mediated Tolerance Induction

Ezh2 expression is frequently reduced in patients with cutaneous allergies (De Benedetto et al., 2011). To determine if Ezh2 expression in skin DCs plays a protective role against cutaneous allergies, we induced CHS, which mimics allergic contact dermatitis in humans, in control mice (*Ezh2$^{f/f}$*) for comparison with animals in which the *Ezh2* gene was deleted only in CD11c$^+$ cells (*CD11c-cre; Ezh2$^{f/f}$*). However, when control animals and *CD11c-cre; Ezh2$^{f/f}$* mice were painted with two consecutive doses of strong hapten 2,4- dinitrofluorobenzene (DNFB) to induce CHS, mice with Ezh2-deficient DCs did not exhibit greater extent of ear swelling than control mice (Figure 1A). We next investigated whether Ezh2 expression in DCs plays a role in the induction of cutaneous tolerance. Here, the mice were tolerized with the weak hapten 2,4-dinitrothiocyanobenzene (DNTB) followed by CHS induction using DNFB (Figure 1B). We observed that tolerization with DNTB was able to suppress the development of DNFB-induced ear swelling in control mice (Figure 1C). In contrast, *CD11c-cre; Ezh2$^{f/f}$* mice developed a robust CHS response that peaked at day 2–3 in spite of prior DNTB treatment, implying an important function of Ezh2-expressing DCs in the induction of cutaneous tolerance (Figure 1C). Consistent with the enhanced ear swelling, analysis of whole-mount ear tissues revealed an accumulation of enlarged DC clusters (Figure 1D), which are indicative of DC activation and enhanced antigen-presenting capacity (Natsuaki et al., 2014). Accordingly, the sdLNs from these animals contained increased numbers of interferon-γ-producing CD8$^+$ T cells with a CD44$^+$ CD62L^{lo} effector or CD44$^+$ CD62L$^+$ central memory phenotype (Figures S1A and S1B). Although we were unable to detect any gross difference in the total numbers of Tregs present in sdLNs between control and *CD11c-cre; Ezh2$^{f/f}$* mice (Figure S1C), a significantly lower proportion of activated Foxp3$^+$ Tregs was found in the sdLNs of DNTB-painted *CD11c-cre; Ezh2$^{f/f}$* mice, as determined by their surface expression of co-stimulatory molecule ICOS (Figures 1E and 1F).

The skin is a complex tissue consisting of multiple phenotypically and functionally heterogeneous CD11c$^+$ DC subsets. To determine which DC subsets contribute to the failed induction of cutaneous tolerance in the *CD11c-cre; Ezh2$^{f/f}$* mice, we took advantage of the radio-resistant feature of LCs and performed a series of reciprocal bone marrow (BM) transplantation experiments to selectively delete Ezh2 in either LCs or dDCs. The complete depletion of recipient origin leukocytes (CD45.2) and the efficient reconstitution of recipient mice with donor cells (CD45.1) were controlled by flow cytometry staining (Figure S1D). Using the same tolerization and sensitization regimen as employed in the previous experiments, we observed an increased ear swelling in BM chimeric mice that lacked Ezh2 only in epidermal LCs (Figure 1G). In contrast, ear inflammation was significantly reduced in BM chimeras whose skin was populated by wild-type LCs and Ezh2-deficient dDCs (Figure 1H). These results suggest that expression of Ezh2 in LCs is required for the induction of cutaneous tolerance.

Ezh2 Is Required for the Migration of Epidermal LCs

As Ezh2 inhibitor-treated leukocytes have been reported to display inflammatory gene signatures (Kruidenier et al., 2012), failure to induce tolerance in *CD11c-cre; Ezh2$^{f/f}$* mice could be the consequence of an

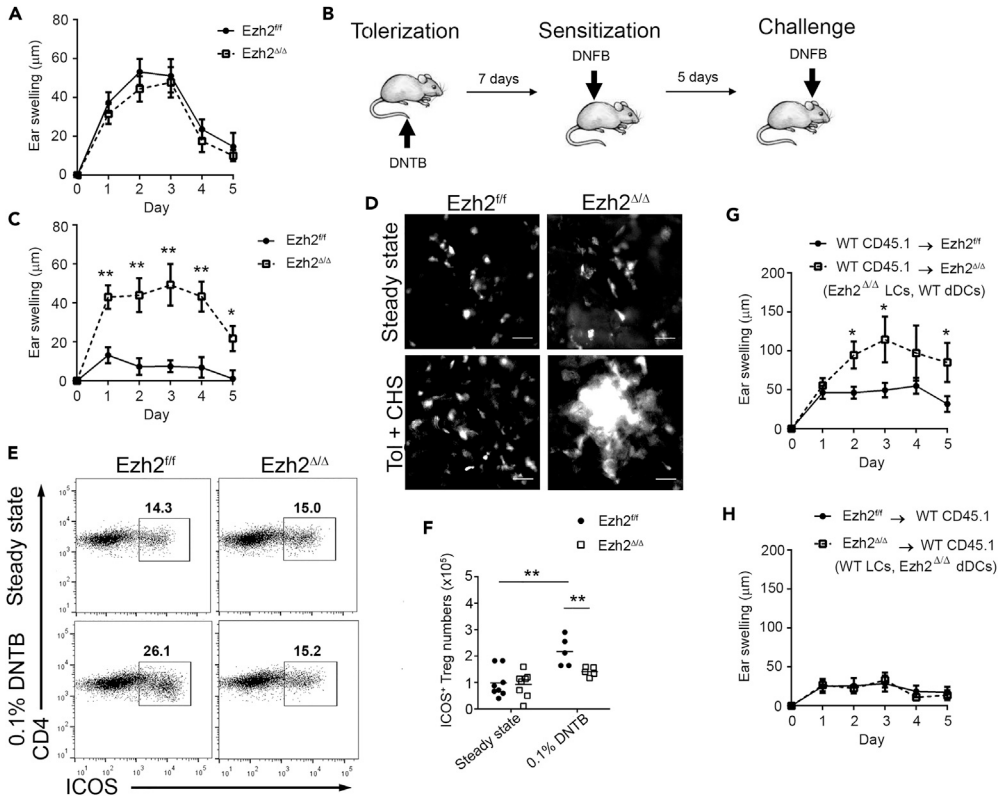

Figure 1. Ezh2-Expressing LCs Induce Cutaneous Tolerance

(A) *Ezh2*$^{f/f}$ (Ezh2$^{f/f}$) or *CD11c-cre; Ezh2*$^{f/f}$ (Ezh2$^{\Delta/\Delta}$) mice were sensitized with 0.5% DNFB on shaved back skin before ear challenge with 0.1% DNFB 5 days later. Ear swelling was determined daily over a period of 5 days post-challenge (mean ± SEM). Data shown are from 2 independent experiments (n = 8).

(B and C) (B) Mice were tolerized with 0.1% DNTB on shaved abdomen skin before treated as described in (A). (C) Ear swelling response was determined daily over a period of 5 days post-challenge (mean ± SEM). Data shown are from 3 independent experiments (n = 9). From left to right *p = 0.01; **p = 0.0002, 0.0005, 0.0006, 0.0004.

(D) *Ezh2*$^{f/f}$*; CD11c-YFP* and *CD11c-cre; Ezh2*$^{f/f}$*; CD11c-YFP* mice were tolerized as described in (B). CD11c-YFP$^+$ dermal DC clustering was visualized in whole-mount ear tissues harvested from untreated steady-state mice or from mice during the elicitation phase of CHS (48 hr after ear challenge with DNFB). Data shown are representative of 3 independent experiments (n = 3). Scale bars, 50 μm.

(E) Mice were tolerized with 0.1% DNTB on shaved abdomen skin, and Treg activation status in sdLNs was determined by flow cytometry on day 5. Dot plots were pre-gated on singlet, live cells, and CD3ε$^+$ CD4$^+$ Foxp3$^+$ Tregs.

(F) Scatterplot indicates absolute number of ICOS$^+$ Tregs in sdLNs of untreated or tolerized mice. Data shown are from 3 independent experiments (n ≥ 5) and were analyzed by two-tailed Student's t test (from left to right; **p = 0.003, 0.01).

(G and H) BM chimeric mice were treated as described in (B), and ear swelling was assessed (mean ± SEM). *Ezh2*$^{f/f}$ and *CD11c-cre; Ezh2*$^{f/f}$ mice are CD45.2. Data were analyzed by two-tailed Student's t test (n > 3) (from left to right *p = 0.02, 0.04, 0.05).

See also Figures S1 and S2.

enhanced inflammatory response by the Ezh2-deficient LCs. To determine if Ezh2 expression in LCs contributes to tolerance induction through classical epigenetic-dependent mechanism, we analyzed global gene expression using RNA sequencing. Surprisingly, control and Ezh2-deficient LCs show similar gene expression profiles (Figure S2A), and in agreement, the global level of tri-methylated H3K27 remained unchanged despite Ezh2 deletion (Figure S2B). This is consistent with our previous report that gene expression profiles are not significantly altered in Ezh2-deficient BM-derived DCs (Gunawan et al., 2015). Hence, it is likely that Ezh2 in LCs promotes tolerance via an epigenetic-independent mechanism.

To further investigate how Ezh2 in LCs mediates cutaneous tolerance, we analyzed the epidermal sheets by immunofluorescence staining. Our data revealed that both control and *CD11c-cre; Ezh2*$^{f/f}$ mice retained a regular network of major histocompatibility complex (MHC) II$^+$ cells with typical LC morphology in the

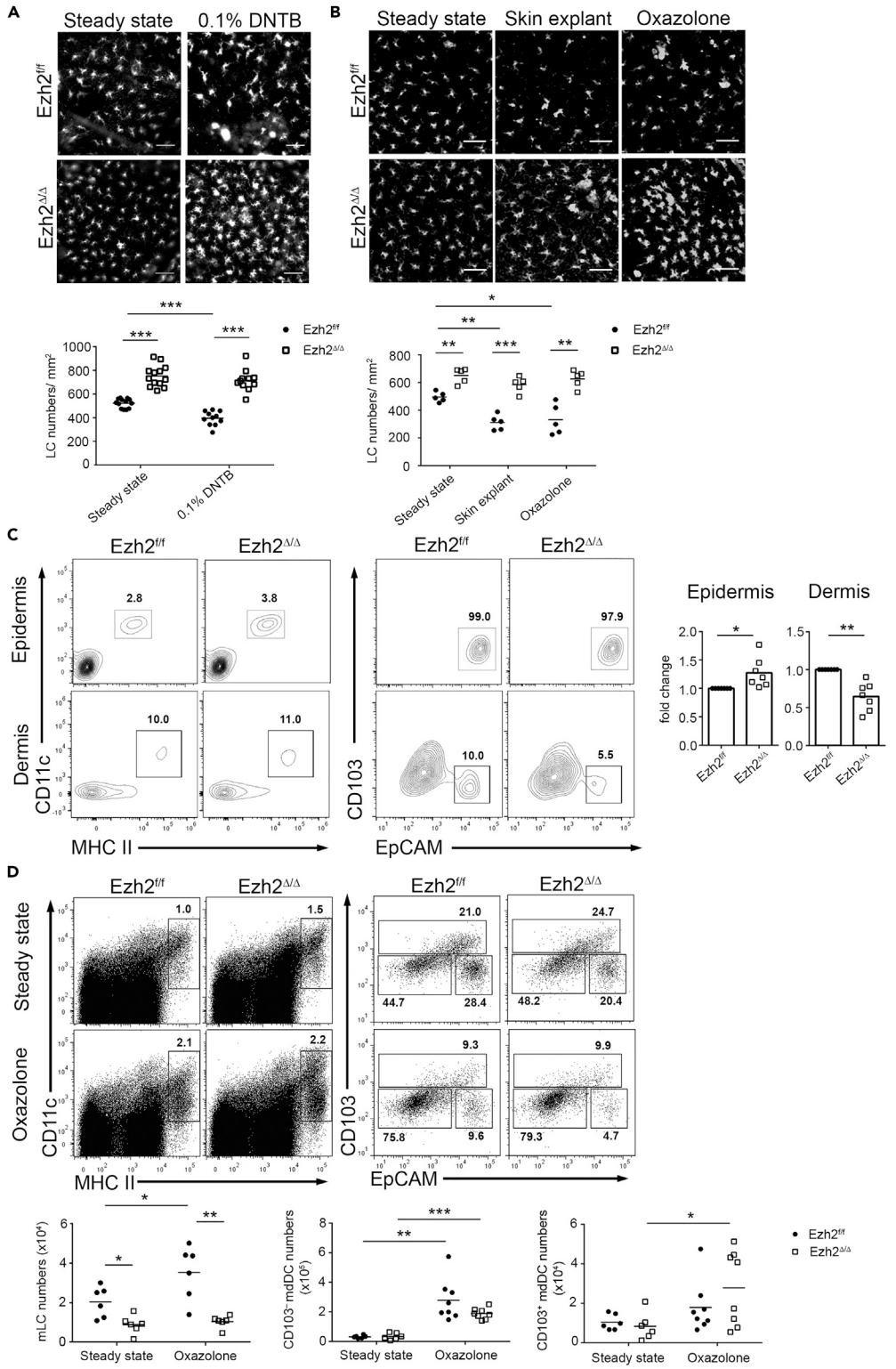

Figure 2. Ezh2 Regulates LC Migration from Epidermis to Skin-Draining Lymph Nodes

(A) Immunofluorescence analysis of epidermal sheets isolated from mouse ears that were treated or not with 0.1% DNTB 18 hr before excision. LCs were identified by immunostaining with anti-MHC II antibody. Images shown are representative of 2 independent experiments (n = 3, total ≥11 fields per group). Scale bars, 50 μm. Scatterplot indicates

Figure 2. *Continued*

LC numbers/mm^2. Data shown are from 2 independent experiments (n = 3, ≥11 fields per group) and were analyzed by two-tailed Student's t test (from left to right ***p = 1.2×10^{-8}, 2.5×10^{-6}, 5.2×10^{-9}).

(B) Immunofluorescence analysis of epidermal sheets isolated from untreated mice (left), cultured for 18 hr in medium (center), or obtained from oxazolone-treated mice 18 hr after application (right). LCs were identified by immunostaining with anti-MHC II antibody. Images shown are representative of 3 independent experiments. Scale bars, 50 μm. Scatterplot indicates LC numbers/mm^2. Data shown are from 3 independent experiments (n = 3, total 5 fields per group) and were analyzed by two-tailed Student's t test (from left to right *p = 0.01; **p = 0.0007, 0.0003, 0.0009; ***p = 5×10^{-5}).

(C) Flow cytometric analyses of LCs in steady-state epidermis and dermis. Contour plots for epidermis are pre-gated on singlet, live cells. Contour plots for dermis were pre-gated on singlet, live, CD45$^+$ cells. CD11c$^+$ MHC II$^+$ DCs were further analyzed for CD103$^-$ EpCAM$^+$ LCs. Data shown are representative of 7 independent experiments. Bar graphs indicate fold-change in percentage of LCs out of total epidermal and dermal cells (percentage of LCs in *Ezh2*$^{f/f}$ mice set as 1). Data shown are from 7 independent experiments (n = 7) and were analyzed by two-tailed Student's t test (*p = 0.01; **p = 0.0003).

(D) 0.5% oxazolone was painted onto mouse ears, and sdLNs were harvested 48 hr later. Dot plots were pre-gated on singlet, live cells. CD11c$^+$ MHC II^{hi} migratory DCs were further analyzed for LCs (CD103$^-$ EpCAM$^+$) and dermal CD103$^-$ and CD103$^+$ DCs (CD103$^{-/+}$ EpCAM$^{-/lo}$). Data shown are representative of 3 independent experiments. Scatterplot indicates the absolute numbers of migratory LCs and dermal CD103$^-$ and CD103$^+$ DCs reaching sdLNs. Data are pooled from 3 independent experiments (n ≥ 6). From left to right *p = 0.01, 0.04, 0.03; **p = 0.001, 0.001; ***p = 9×10^{-7}.

See also Figures S3 and S4.

epidermis (Figure 2A). However, when we quantified resident LC numbers, we detected an increased density of Ezh2-deficient LCs in the untreated epidermis (Figure 2A, left, steady state). As adult LCs are derived from embryonic precursors that take residence in fetal skin *in utero* and undergo a proliferative burst shortly after birth (Hoeffel et al., 2012), we next assessed whether steady-state accumulation of epidermal LCs in *CD11c-cre; Ezh2*$^{f/f}$ mice could be due to differential proliferation of Ezh2-deficient CD11c$^+$ precursors. However, when we evaluated LC density in 2-week-old mice, we observed no significant difference between control animals and *CD11c-cre; Ezh2*$^{f/f}$ mice. Instead, Ezh2-deficient LCs accumulated gradually in the epidermis with increasing age (Figures S3A and S3B), whereas the numbers of proliferating and apoptotic LCs in these mice were comparable to that in the control mice (Figures S3C–S3H), suggesting that Ezh2 expression in LCs could be critical for their steady-state emigration from the epidermis. It is likely that Ezh2-deficient LCs fail to emigrate from the epidermis upon DNTB application and thereby contribute to defective tolerance induction. Indeed, whereas control LCs migrated away from the epidermis in response to DNTB painting, Ezh2-deficient LCs were unable to exit the skin when exposed to the same treatment (Figure 2A, right, 0.1% DNTB). These data suggest that Ezh2 is likely to be required for the induction of cutaneous tolerance by regulating LC migration away from the epidermis.

We further verify the importance of Ezh2 in regulating LC migration using skin explant culture and oxazolone skin sensitization models. Similarly, whereas control LCs efficiently migrated away from the skin explants or oxazolone-painted skin, Ezh2-deficient LCs persisted in the epidermis despite exposure to these potent activating stimuli (Figure 2B). Flow cytometry analysis also revealed a reduction in migratory LCs (MHC II^{hi} CD11c$^+$ EpCAM$^+$ CD103$^-$ cells) in the dermal layers (Figure 2C) and sdLNs of untreated *CD11c-cre; Ezh2*$^{f/f}$ mice (Figure 2D), indicating a defect in their steady-state migration. Moreover, even though oxazolone sensitization induced a robust migration of control LCs to sdLNs within 48 hr of administration, this treatment failed to increase LC numbers in sdLNs of *CD11c-cre; Ezh2*$^{f/f}$ mice (Figure 2D). In contrast to LCs, migration of dDCs (MHC II^{hi} CD11c$^+$ EpCAM$^-$ CD103$^{-/+}$ cells) to sdLNs was not altered by Ezh2 deficiency either under steady-state conditions or following oxazolone sensitization (Figure 2D). In addition, we found a marked up-regulation of Ezh2 mRNA and protein expression in migratory LCs isolated from sdLNs compared with epidermis-resident LCs (Figures S3I and S3J), further supporting a role of Ezh2 in controlling LC localization and function. Together, these data strongly indicate that Ezh2 is required for LC migration away from the epidermis under both steady-state and immunostimulatory conditions.

To determine whether our findings are relevant in the human context, we analyzed LC migration from human skin treated with GSK126, a small molecule inhibitor of Ezh2 methyltransferase activity (McCabe et al., 2012). Indeed, co-culture of human skin explants with GSK126 resulted in a decline in LC migration, in which we observed a decrease in emigrated LCs present in the tissue culture medium (Figures 3A–3C) and a concomitant increase in LCs remaining in the epidermal sheet (Figure 3D). Hence, in agreement with our mouse model, our studies using human skin explants suggest that Ezh2's methyltransferase activity is also required for human LC migration away from the epidermis.

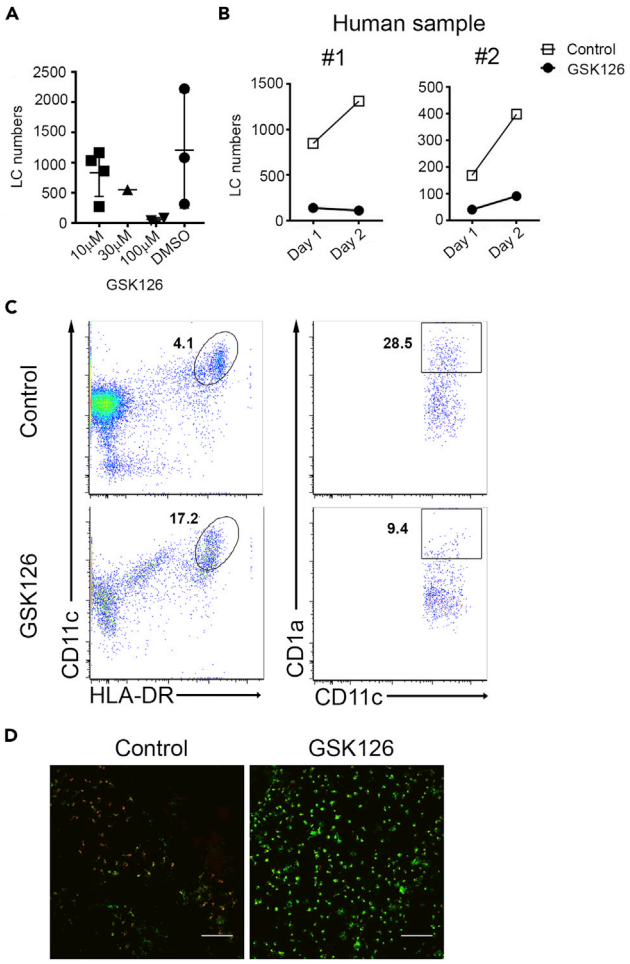

Figure 3. Ezh2 Regulates Migration of Human LCs

(A) Human skin explants were cultured overnight in medium containing DMSO (control) or increasing concentrations of GSK126. Cells were retrieved from the culture medium, and LCs were identified by flow cytometry. Graph indicates numbers of LCs retrieved from the culture medium (n > 3).

(B) Skin explants from 2 independent human samples were cultured for 2 days in medium containing DMSO (control) or 100 μM of GSK126. Cells were retrieved from the medium following 1 or 2 days of culture, and LCs were identified by flow cytometry. Graph indicates numbers of LCs retrieved from the culture medium (n = 2).

(C) Cells retrieved from the medium in (B) were analyzed by flow cytometry. Dot plots were pre-gated on $CD45^+$ cells. $CD11c^+$ $HLA\text{-}DR^+$ DCs were further analyzed for CD1a expression to define LCs.

(D) Epidermal sheets were isolated from human skin explants in (B) and stained with anti-HLA-DR (green) and anti-Langerin (red). Scale bars, 100 μm.

See also Figure S4.

Ezh2 Regulates LC Transmigration across the Basement Membrane

In order for LCs to reach the dermis and sdLNs, they must disengage from their epidermal niche before crossing the underlying basement membrane, which is primarily composed of a dense network of type IV collagen and laminin (Yurchenco, 2011). It is possible that trapping of Ezh2-deficient LCs in the epidermis is due to dysregulated expression of adhesion/migration-related molecules that anchor LCs to the surrounding keratinocytes. We therefore examined LC expression of molecules that have been reported to govern emigration from the epidermis, namely, E-cadherin, integrin α6, and CXCR4 (Price et al., 1997; Tang et al., 1993; Villablanca and Mora, 2008). In particular, E-cadherin was previously identified as a target gene of Ezh2-mediated epigenetic silencing in various cancer cells (Cao et al., 2008). However, the expression of these proteins in LCs during steady state and upon activation were not affected by Ezh2 deficiency (Figures S4A–S4C), which is in accordance with the comparable gene expression profiles of control and Ezh2-deficient LCs (Figure S2A). Lack of major changes in overall gene expression profiles is perhaps

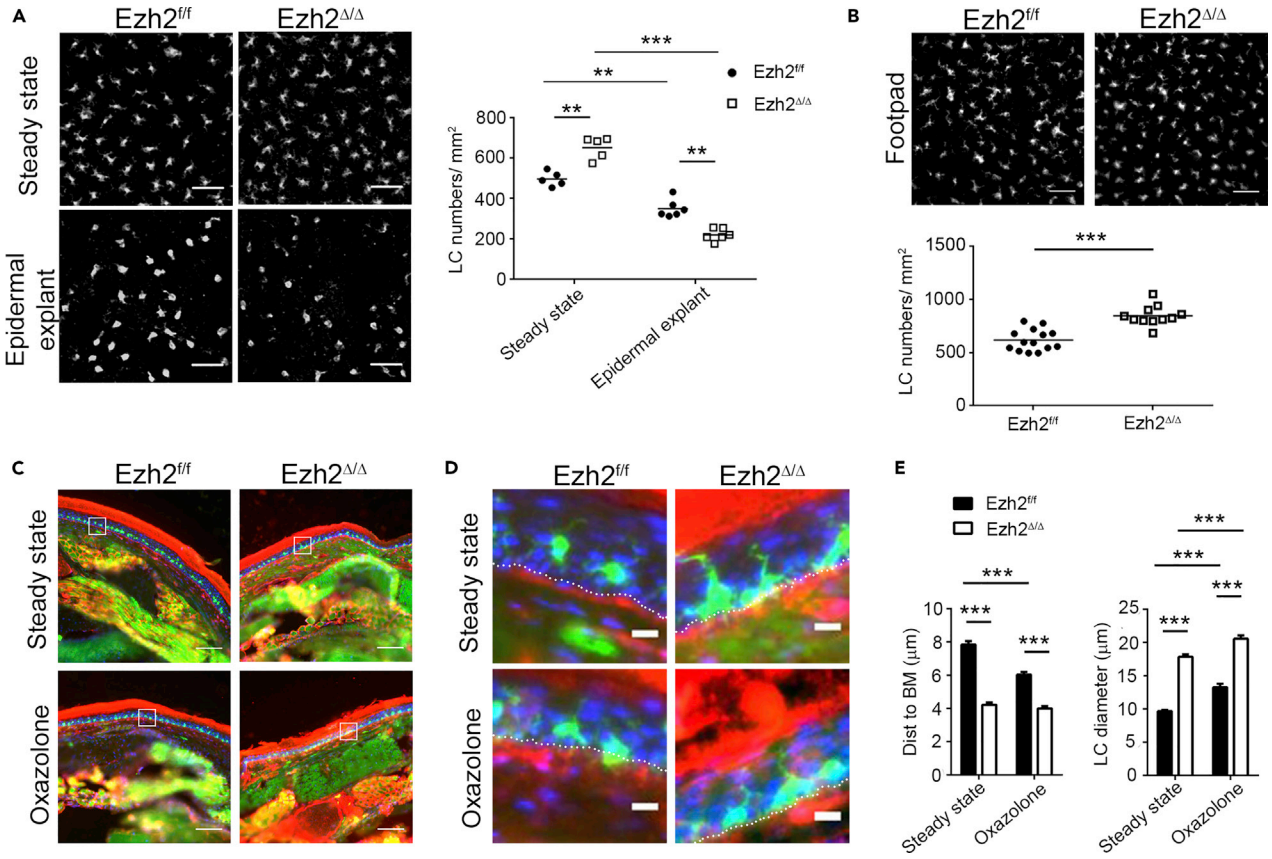

Figure 4. Ezh2 Regulates LC Transmigration across Basement Membrane

(A) Epidermal sheets were isolated by dispase digestion, and then cultured for 4 hr before staining with anti-MHC II antibody. Images shown are representative of 2 independent experiments (n = 3, total ≥5 fields per group). Scale bars, 50 μm. Scatterplot indicates LC numbers/mm^2. Data shown are from 2 independent experiments (n = 3, total ≥5 fields per group) and were analyzed by two-tailed Student's t test (from left to right **p = 0.0007, 0.0002, 0.0002; ***p = 4 × 10^{-6}).

(B) Immunofluorescence analysis of epidermal sheets isolated from untreated footpads. Images shown are representative of 2 independent experiments (n = 3, total ≥11 fields per group). Scale bars, 50 μm. Scatterplot indicates LC numbers/mm^2. Data shown are from 2 independent experiments (n = 3, total ≥11 fields per group) and were analyzed by two-tailed Student's t test (***p = 6 × 10^{-6}).

(C and D) 0.5% oxazolone was painted onto footpad skin before harvesting 18 hr later. Untreated and oxazolone-painted footpad skin sections were stained with anti-laminin (red) and DAPI (blue). Endogenous CD11c-YFP$^+$ LCs are visualized in green. Images shown are representative of 3 independent experiments (n = 3). Scale bars, 100 μm. Boxes outlined in (C) are enlarged in (D); scale bars, 10 μm in (D).

(E) Bar graph quantification of images in (C), showing distance of epidermal LCs (green) from the basement membrane (red) and LC diameter during steady state and after oxazolone administration (mean ± SEM of more than 200 cells per group). Data were analyzed by two-tailed Student's t test (from left to right ***p = 1 × 10^{-41}, 1 × 10^{-11}, 8 × 10^{-20}, 6.5 × 10^{-51}, 1.4 × 10^{-10}, 4.5 × 10^{-5}, 2.8 × 10^{-21}).

See also Figure S4.

due to the compensatory effects of alternative histone methyltransferases. Indeed, the expression of a closely related histone methyltransferase—Ezh1, which shares some target genes with Ezh2 (Margueron et al., 2008; Shen et al., 2008), was increased in Ezh2-deficient BM-derived DCs (Figure S4D). Together, these results suggest that impaired migration of Ezh2-deficient LCs is not due to dysregulated expression of molecules involved in cell adhesion/migration.

We next investigated whether basement membrane represents a physical barrier that blocks transmigration of Ezh2-deficient LCs into the dermis. We first subjected excised skin samples to dispase digestion and cultured the isolated epidermis to facilitate LC activation *in vitro*. Dispase can disrupt the integrity of the basement membrane via specific cleavage of type IV collagen in the lamina densa, while leaving the epidermis intact (Stenn et al., 1989). In the absence of an intact basement membrane, activated Ezh2-deficient LCs were able to migrate away from epidermal sheet explants (Figures 4A and S4E). The observed reduction in epidermal LCs in this setting was not caused by increased cell death, as we

recovered similar percentages of total viable LCs from both control and Ezh2-deficient tissue culture medium in these experiments (Figure S4F).

To further assess the importance of Ezh2 in regulating LC transmigration *in vivo*, we examined mouse skin by sectioning to visualize the longitudinal distribution of LCs throughout the epidermis. For these analyses, we used footpad rather than ear skin to obtain better resolution between the epidermal layer and basement membrane. Similar to our previous observations in ear skin, we detected a significant steady-state accumulation of epidermal LCs in footpad from *CD11c-cre; Ezh2$^{f/f}$* mice (Figure 4B). Transverse sections of the untreated footpad revealed that the majority of control LCs displayed rounded morphology and were evenly distributed among the keratinocytes ~8 μm above the basement membrane (Figures 4C–4E). Upon contact sensitization with oxazolone, these LCs became activated and were observed to migrate toward the basement membrane (Figures 4C–4E) and occasionally extend dendrites and/or cell body through into the dermis (Figure 4D). In contrast, Ezh2-deficient LCs were frequently found to line up against the basement membrane with atypical flattened morphology, with increased cell spreading upon activation with oxazolone (Figures 4C–4E). This apparent defect in transmigration of Ezh2-deficient LCs across the basement membrane could not be attributed to decreased matrix metalloproteinase (MMP) activity (Figures S4G and S4H) or increased expression of tissue inhibitors of MMP 2 and 3 (Figure S4I), which are reported target genes of Ezh2 in cancer cells (Shin and Kim, 2012; Xu et al., 2013). Taken together, these data reveal that Ezh2-deficient LCs are unable to transmigrate across the basement membrane to exit the skin.

Ezh2 Controls Adhesion Dynamics and Migration of LCs

We have previously reported that cytosolic Ezh2 acts on the extranuclear substrate Talin1 by catalyzing the addition of three methyl groups at Lys 2454 to disrupt binding to F-actin (Gunawan et al., 2015; Venkatesan et al., 2018). As Talin1 is a critical component of the focal adhesion complex (Franco et al., 2004), we hypothesized that Ezh2-mediated methylation of Talin1 contributes to the transmigration of LCs across the basement membrane. To test this possibility, we next isolated LCs for *ex vivo* assessment of their ability to attach to a laminin-coated surface that mimics the basement membrane *in vivo*. Immunostaining revealed that the majority of control LCs did not form notable adhesion structures in these assays, whereas Ezh2-deficient LCs frequently formed numerous and enlarged adhesion structures upon attachment to laminin (Figures 5A–5C). It is likely that Ezh2 regulates the turnover of adhesion structures in LCs via methylation of Talin1, similar to our previous observations in BM-derived DCs (Gunawan et al., 2015).

Moreover, consistent with our findings in longitudinal skin sections, Ezh2-deficient LCs tended to exhibit excessive spreading upon interaction with laminin, which gave rise to an increased surface area ~2-fold greater than that of control LCs (Figures 5A and 5D). Consequently, when we evaluated the migratory capacity of LCs on a laminin-coated surface via time-lapse imaging, we observed that Ezh2-deficient LCs appeared tightly adhered and were largely immobile, whereas control cells were highly migratory under the same conditions (Figures 5E and 5F). We next assessed whether this migration defect in Ezh2-deficient LCs was due to an inability to methylate Talin1 at Lys 2454. To do this *in vivo*, we analyzed the adhesion dynamics and migratory capacity of LCs in mouse skin infected with retrovirus to express various Talin1 mutants (Figure S5A). Substitution of K2454 with a glutamine (K2454Q) residue that cannot undergo methylation resulted in impaired migration of control LCs away from the epidermis to sdLNs in response to oxazolone treatment similar to the Ezh2-deficient LCs (Figures 5G, 5H, and S5B). In contrast, replacement of K2454 with the methyl-mimicking residue phenylalanine (K2454F) restored the migratory capacity of Ezh2-deficient LCs (Figures 5G, 5H, and S5B). Consequently, Ezh2-deficient LCs expressing Talin1-K2454F were now able to reach the sdLNs at a comparable rate as control cells, whereas cells expressing wild-type Talin1 or Talin1-K2454Q were trapped in the epidermis (Figures 5G, 5H, and S5B). These data were consistent with our earlier *in vitro* observation that Talin1 methylation promotes turnover of adhesion structures and enhances cell migration, whereas unmethylatable Talin1 renders cells immobile (Gunawan et al., 2015). Taken together, these findings suggest that Ezh2 regulates LC transmigration across basement membrane via a non-epigenetic mechanism involving the methylation of Talin1 and subsequently affects the turnover of adhesion structures.

Mobilization of Ezh2-Deficient Dermal DCs with Enhanced Tolerogenic Activity Restores Cutaneous Tolerance

Our findings reported above indicate that Ezh2 regulates LC transmigration across basement membrane during induction of cutaneous tolerance. As other dDC subsets have also been implicated in tolerance

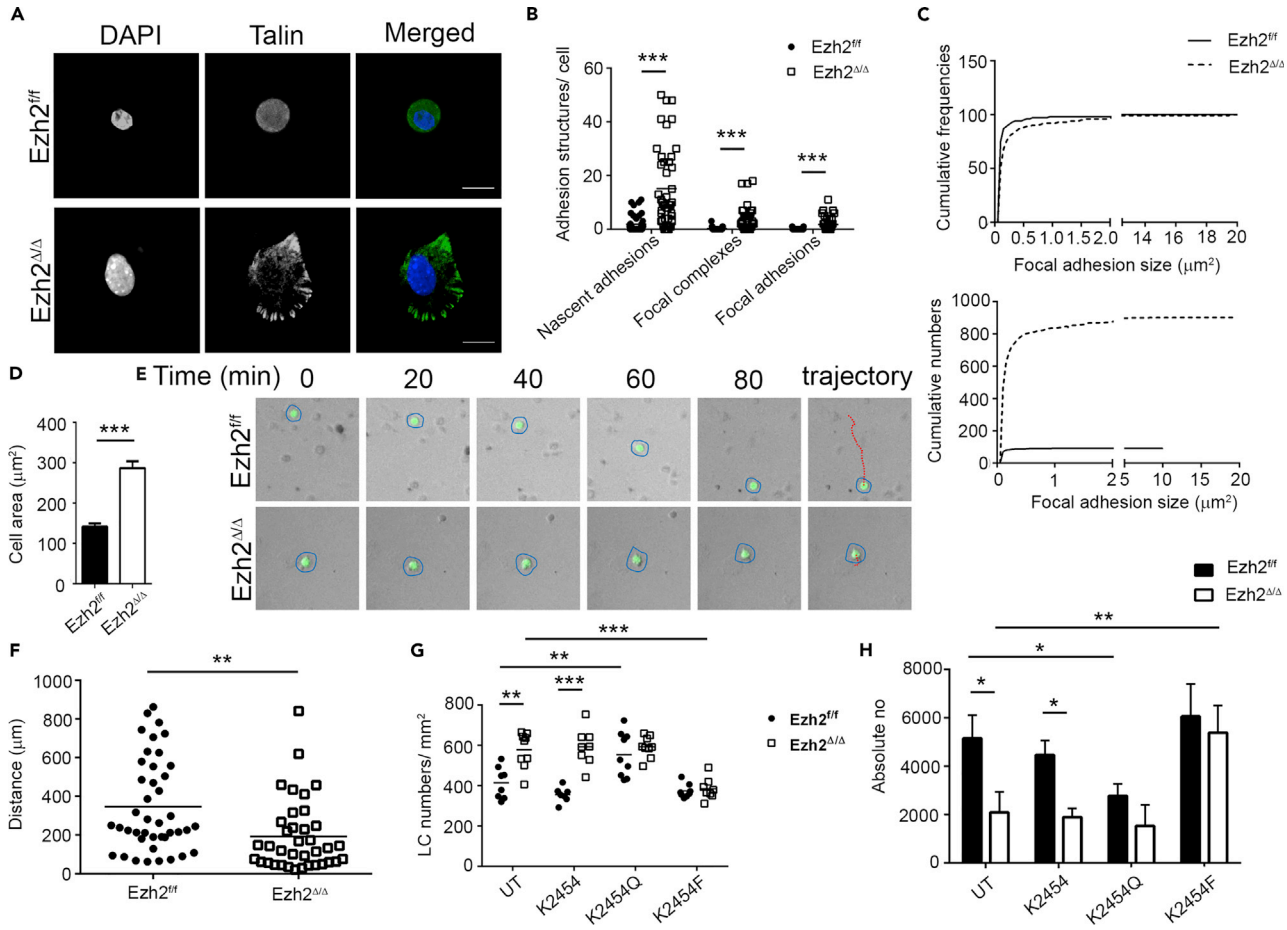

Figure 5. Ezh2 Regulates Adhesion Characteristics of Skin LCs

(A) LCs attached on laminin-coated slides were immunostained with DAPI (blue) and anti-Talin antibody (green). Images are representative of 4 independent experiments (n = 4). Scale bars, 10 μm.

(B) Scatterplot indicates distribution of adhesion structures in LCs. Data shown are from 4 independent experiments (n = 4) and were analyzed by two-tailed Student's t test (from left to right ***p = 5×10^{-7}, 1×10^{-5}, 3×10^{-5}).

(C) Cumulative frequencies and numbers of adhesion structures as in (B). Data shown are from 4 independent experiments and were analyzed by Kolmogorov-Smirnov test (p = 1.4×10^{-9}).

(D) Bar graph indicates surface area of LCs from (A) (mean ± SD). Data shown are from 4 independent experiments (n = 4) and were analyzed by two-tailed Student's t test (***p = 2×10^{-12}).

(E and F) (E) Migration of CD11c-YFP^{+} LCs (green/outlined) on laminin-coated slides was tracked by time-lapse imaging. (F) Scatterplot indicates total distance moved by LCs in (E). Data shown are from 4 independent experiments (n = 4, 42 control and 35 Ezh2-deficient cells pooled from 4 experiments were scored). (**p = 0.002).

(G and H) Mouse ears were tape-stripped and infected with retroviral vector carrying different GFP-tagged Talin1 mutants (K2454, K2454Q, K2454F). 0.5% oxazolone was painted onto untransduced (UT) or retrovirus-infected mouse ears, and epidermis and sdLNs were harvested 18 and 48 hr later respectively. (G) Scatterplot indicates epidermal LC numbers/mm^2. Data shown are from 3 independent experiments (n = 3, ≥7 fields per group) and were analyzed by two-tailed Student's t test (from left to right **p = 0.001, 0.009; ***p = 2.5×10^{-5}, 7.8×10^{-5}). (H) Bar graph indicates absolute number of LCs reaching sdLNs (mean ± SEM). Data shown are from 2 independent experiments (n = 3) and were analyzed by two-tailed Student's t test (from left to right *p = 0.03, 0.05, 0.02; **p = 0.009).

See also Figure S5.

induction, and our study revealed that migration of dDCs to sdLNs was unaffected by Ezh2 deficiency upon contact sensitization with oxazolone (Figure 2D), we were intrigued by the failed cutaneous tolerance induction observed in *CD11c-cre; Ezh2$^{f/f}$* mice (Figure 1C), in which only the migration of LCs was impaired. Thus we investigated the migratory DC populations in sdLNs and observed that LCs was the only population to be mobilized to the sdLNs upon DNTB application in our experimental setting (Figures 6A and 6B). As high dosage of haptens has been shown to disseminate into the dermis enabling mobilization of dDCs (Noordegraaf et al., 2010), we treated control and *CD11c-cre; Ezh2$^{f/f}$* mice with a 10-fold higher dose of

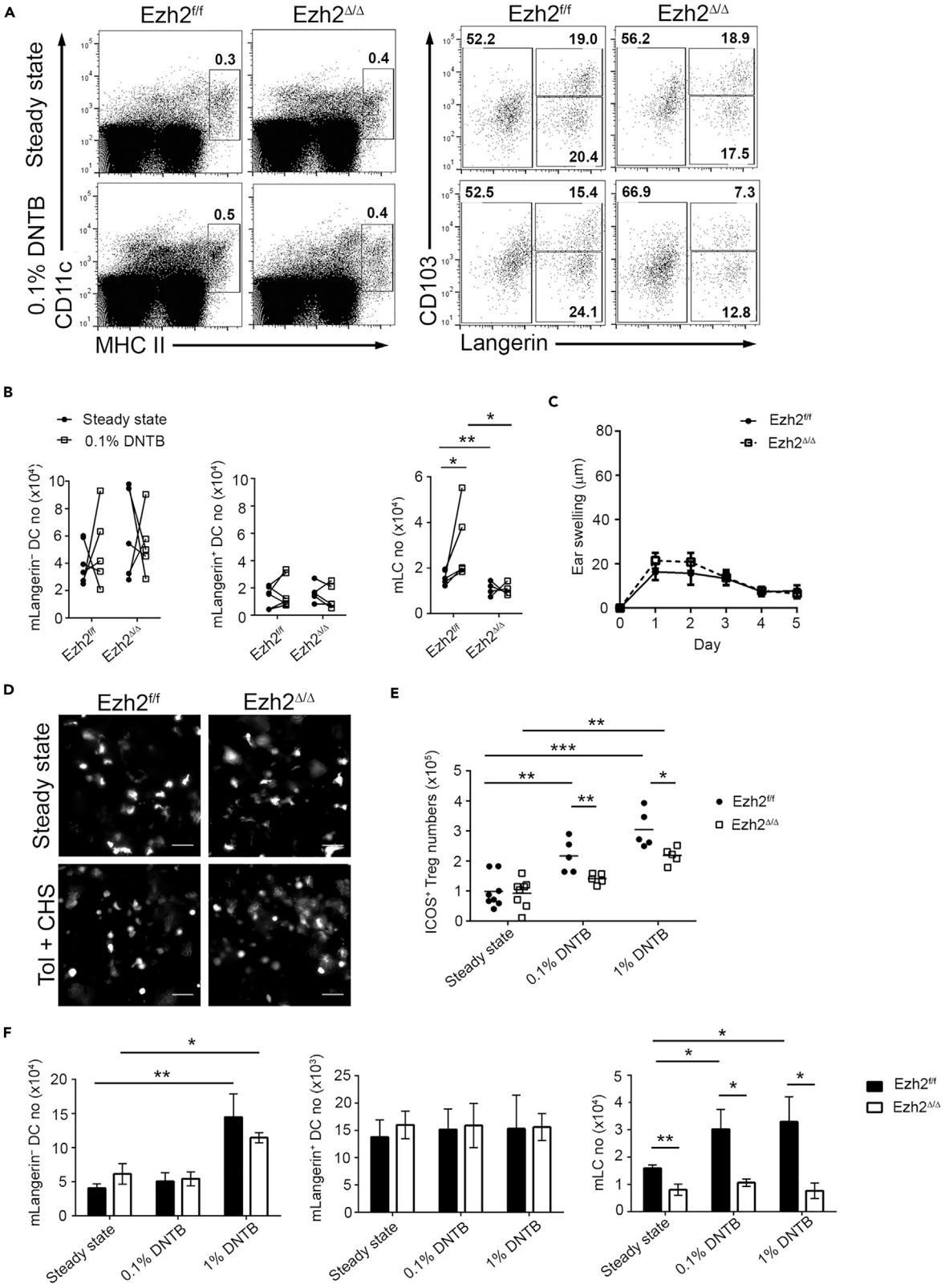
A
Ezh2f/f
Ezh2Δ/Δ
Steady state
0.1% DNTB
CD11c
MHC II
0.3
0.4
0.5
0.4
CD103
Langerin
52.2
19.0
20.4
56.2
18.9
17.5
52.5
15.4
24.1
66.9
7.3
12.8
B
Steady state
0.1% DNTB
mLangerin- DC no (x10⁴)
mLangerin+ DC no (x10⁴)
mLC no (x10⁴)
C
Ear swelling (μm)
Day
D
Tol + CHS
E
ICOS+ Treg numbers (x10⁵)
Steady state
0.1% DNTB
1% DNTB
F
mLangerin- DC no (x10⁴)
mLangerin+ DC no (x10³)
mLC no (x10⁴)

Figure 6. Dermal DCs Exposed to High-Dose DNTB Restore Tolerance in *CD11c-cre; Ezh2$^{f/f}$* Mice

(A) Flow cytometric analyses of migratory DCs in sdLNs from mice that were tolerized with or without 0.1% DNTB 48 hr prior. Dot plots were pre-gated on singlet, live cells. CD11c^{+} MHC II^{hi} migratory DCs were further analyzed for Langerin^{+} CD103^{-} LCs, Langerin^{+} CD103^{+} dermal DCs, and Langerin^{-} dermal DCs. Data shown are representative of 4 independent experiments ($n \geq 5$).

(B) Scatterplot indicates absolute numbers of migratory DCs recovered from sdLNs of untreated and DNTB-painted mice. Data shown are from 4 independent experiments ($n \geq 5$) and were analyzed by two-tailed Student's t test (from left to right *p = 0.05, 0.04; **p = 0.007).

(C) Mice were tolerized with 1% DNTB on shaved abdomen skin before treated as described in Figure 1A. Ear swelling response was determined daily over a period of 5 days (mean ± SEM). Data shown are from 2 independent experiments ($n \geq 8$).

(D) CD11c-YFP^{+} dermal DC clustering was visualized in whole-mount ear tissues 48 hr after DNFB challenge. Data shown are representative of 3 independent experiments (n = 3). Scale bars, 50 μm.

(E) Scatterplot indicates absolute numbers of ICOS^{+} Tregs in sdLNs from untreated mice or mice tolerized with 0.1% or 1% DNTB. Data shown are from 3 independent experiments ($n \geq 5$) and were analyzed by two-tailed Student's t test (from left to right *p = 0.02; **p = 0.003, 0.01, 0.0002; ***p = 6.1×10^{-5}).

(F) Bar graphs indicate absolute numbers of migratory DCs reaching sdLNs of untreated mice or mice treated with 0.1% or 1% DNTB (mean ± SEM). Data shown are from 4 independent experiments ($n \geq 5$) and were analyzed by two-tailed Student's t test (from left to right *p = 0.02, 0.05, 0.05, 0.04, 0.04; **p = 0.01, 0.007).

DNTB. Interestingly, at high-dose DNTB (1%), we were able to restore tolerance in *CD11c-cre; Ezh2$^{f/f}$* mice as indicated by reduced ear swelling (Figure 6C) and attenuated formation of dDC clusters (Figure 6D). An expansion of activated ICOS^{+} Tregs was also observed in the sdLNs of *CD11c-cre; Ezh2$^{f/f}$* mice, and this number was comparable to that observed in the control mice treated with low-dose DNTB (0.1%) (Figure 6E). This effect was associated with an increased number of migratory Langerin^{-} dDCs (MHC II^{hi} CD11c^{+} CD103^{-} CD11b^{+}), whereas the number of Langerin^{+} dDCs remained unchanged in both control and *CD11c-cre; Ezh2$^{f/f}$* mice (Figure 6F). Moreover, upon high-dose DNTB treatment, Ezh2-deficient LCs were still trapped in the epidermis and the number of migratory LCs in sdLNs remained low (Figure 6F). These results suggest that upon treatment with a high dosage of haptens, Ezh2-deficient Langerin^{-} dDCs are able to compensate for the reduced LC numbers in sdLNs of *CD11c-cre; Ezh2$^{f/f}$* mice to promote tolerance.

Even though Langerin^{-} dDCs have been reported to harbor ALDH activity required for Treg differentiation (Guilliams et al., 2010), they are unable to promote DNTB-mediated cutaneous tolerance in the absence of LCs (Gomez de Aguero et al., 2012). As increased numbers of migratory Ezh2-deficient Langerin^{-} dDCs in sdLNs were correlated with restored tolerance in the absence of inflammation-induced migratory LCs (Figures 6C, 6E, and 6F), Ezh2-deficient Langerin^{-} dDCs are likely to exhibit higher tolerogenic capacity than control counterparts. In fact, even though the overall H3K27me3 levels were comparable between control and Ezh2-deficient DCs and our previous microarray analysis did not show a major difference in gene expression patterns, *Aldh2* is among a handful of up-regulated genes in Ezh2-deficient DCs (Gunawan et al., 2015). Therefore, we further investigated ALDH activity and found that a higher percentage of Ezh2-deficient CD11b^{+} dDCs (Langerin^{-} dDC-equivalent cell population) exhibited ALDH activity than control cells (Figures 7A and 7B). A similar increase was observed in Ezh2-deficient BM-derived DCs after lipopolysaccharide stimulation (Figures 7C and 7D, mature). Treatment of BMDCs with diethylaminobenzaldehyde, an inhibitor of ALDH activity, was included to determine the specificity of AldeFluor staining (Figure 7C). Moreover, the expressions of ALDH protein and mRNAs were also higher in Ezh2-deficient BMDCs than in control cells (Figures 7E and 7F). Next, to determine whether Ezh2 regulates ALDH expression and activity via the classical epigenetic-dependent mechanism, we performed chromatin immunoprecipitation in BMDCs with an antibody recognizing tri-methylated H3K27 (H3K27me3) and observed that the association of H3K27me3 with the *Aldh1* or *Aldh2* promoters in control cells (Figure 7G). The amount of H3K27me3 associated with these promoters was significantly reduced in Ezh2-deficient DCs (Figure 7G), which is consistent with the reduced transcriptional repression of *Aldh* genes and increased number of cells with ALDH activity. Taken together, these data reveal that upon exposure to a high-dose hapten, Ezh2-deficient Langerin^{-} dDCs, which express high level of ALDH, are efficiently mobilized and are likely to substitute LCs in promoting cutaneous tolerance.

DISCUSSION

Here we have reported that Ezh2 controls skin tolerance by regulating different subsets of skin DCs via distinct mechanisms. Ezh2 is required for the regulation of LC transmigration across epidermal basement membrane via direct methylation of Talin1 and thereby promotes adhesion turnover, consequently affecting tolerance induction against cutaneous allergens. Moreover, we also identify a subset of Ezh2-deficient dDCs with enhanced ALDH activity, which could potentially rescue tolerance when LCs are unable to exit the skin compartment. These data reveal previously unappreciated abilities of Ezh2 to regulate LC

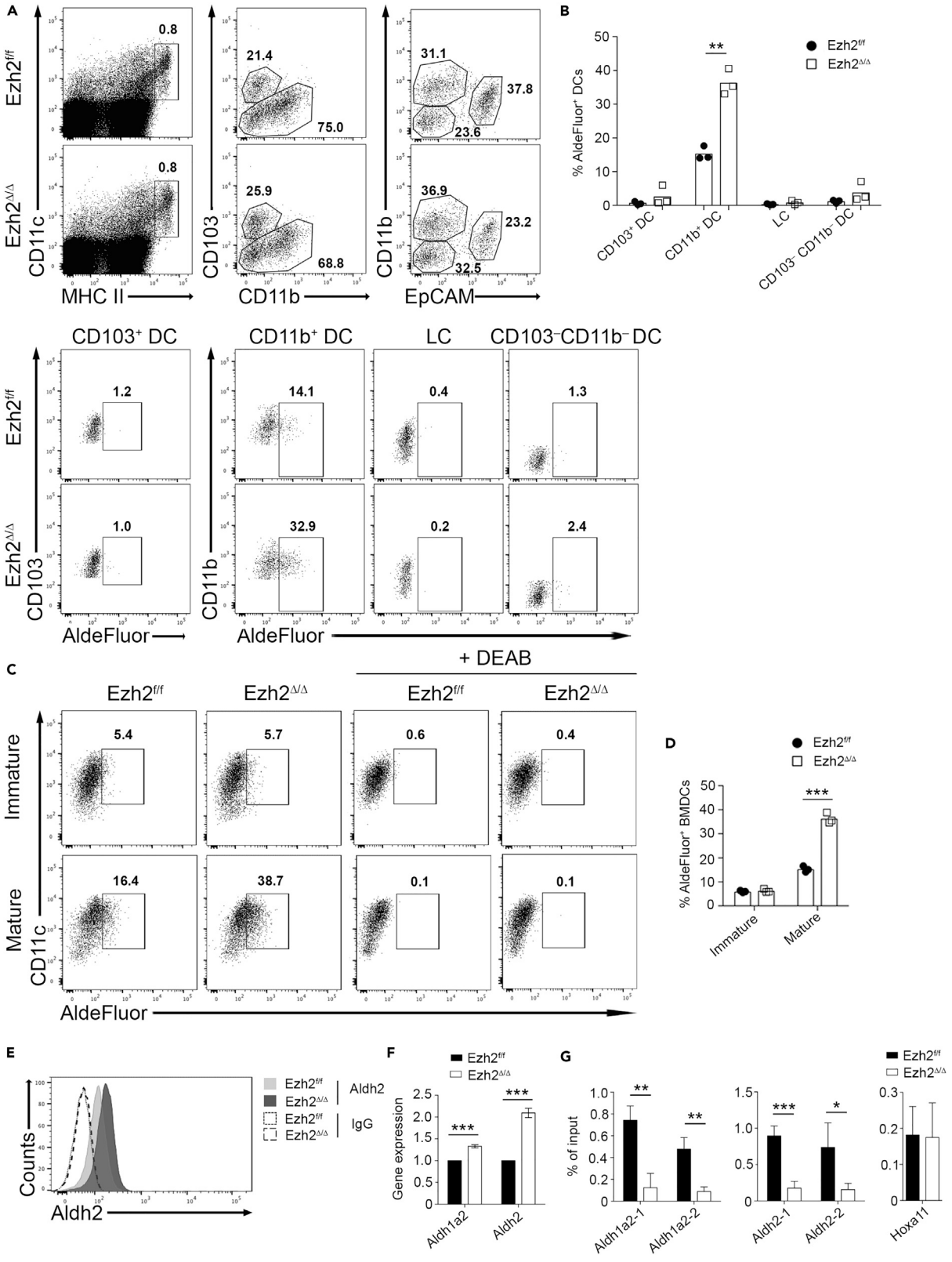
A
Ezh2f/f
Ezh2Δ/Δ
CD11c
MHC II
0.8
0.8
CD103
CD11b
21.4
75.0
25.9
68.8
CD11b
EpCAM
31.1
37.8
23.6
36.9
23.2
32.5
B
% AldeFluor+ DCs
Ezh2f/f
Ezh2Δ/Δ
**
CD103+ DC
CD11b+ DC
LC
CD103− CD11b− DC
CD103+ DC
CD11b+ DC
LC
CD103−CD11b− DC
Ezh2f/f
Ezh2Δ/Δ
CD103
CD11b
AldeFluor
1.2
14.1
0.4
1.3
1.0
32.9
0.2
2.4
C
+ DEAB
Ezh2f/f
Ezh2Δ/Δ
Ezh2f/f
Ezh2Δ/Δ
Immature
Mature
CD11c
AldeFluor
5.4
5.7
0.6
0.4
16.4
38.7
0.1
0.1
D
Ezh2f/f
Ezh2Δ/Δ
% AldeFluor+ BMDCs
***
Immature
Mature
E
Counts
Aldh2
Ezh2f/f
Ezh2Δ/Δ
Aldh2
Ezh2f/f
Ezh2Δ/Δ
IgG
F
Ezh2f/f
Ezh2Δ/Δ
Gene expression
***
***
Aldh1a2
Aldh2
G
Ezh2f/f
Ezh2Δ/Δ
% of input
**
**
***
*
0.3
0.2
0.1
0
Aldh1a2-1
Aldh1a2-2
Aldh2-1
Aldh2-2
Hoxa11

Figure 7. Ezh2 Represses Aldehyde Dehydrogenase Activity of Dendritic Cells

(A) ALDH activity of individual DC subsets in sdLNs. Dot plots were pre-gated on singlet, live cells. CD11c^{+} MHC II^{hi} migratory DCs were further analyzed for CD103^{+} DCs (CD103^{+} CD11b$^{-/+}$), CD11b^{+} DCs (CD103^{-} CD11b^{+} EpCAM^{-}), LCs (CD103^{-} CD11b^{+} EpCAM^{+}), and CD103^{-} CD11b^{-} DCs (CD103^{-} CD11b^{-} EpCAM^{-}) (top panel). Data shown are representative of 3 independent experiments.

(B) Bar graphs indicate percentages of AldeFluor^{+} cells. Data shown are from 3 independent experiments (n = 3) and were analyzed by two-tailed Student's t test (**p = 0.001).

(C) ALDH activity of immature and mature BMDCs. Cells treated with ALDH inhibitor (diethylaminobenzaldehyde) were included to determine specificity of staining. Dot plots were pre-gated on singlet, live cells. Data shown are representative of 3 independent experiments (n = 3).

(D) Bar graph indicates percentages of AldeFluor^{+} cells. Data shown are from 3 independent experiments (n = 3) and were analyzed by two-tailed Student's t test (***p = 0.0001).

(E) Expression of Aldh2 in mature BMDCs by intracellular staining. Data shown are representative of 3 independent experiments (n = 3).

(F) *Aldh1a2* and *Aldh2* expression in control and Ezh2-deficient mature BMDCs (mean ± SEM). Gene expression was normalized against *Hprt*. Data shown are representative of 3 independent experiments (n = 3) and were analyzed by two-tailed Student's t test (from left to right ***p = 0.0001, 0.0001).

(G) H3K27me3 chromatin immunoprecipitation assay of *Aldh1a2* and *Aldh2* in mature control and Ezh2-deficient BMDCs (mean ± SEM). *Hoxa11* is included as a non-target control. Primer sets 1 and 2 for both *Aldh* genes are located distal and proximal to the transcription start sites, respectively. Data shown are representative of 3 independent experiments (n = 3) and were analyzed by two-tailed Student's t test (from left to right *p = 0.02; **p = 0.0006, 0.0005; ***p = 0.0001).

migration non-epigenetically and ALDH activity of DCs epigenetically, which collectively contribute to its role in controlling cutaneous tolerance.

Ezh2 is a well-established histone methyltransferase that mediates gene silencing via regulation of chromatin compaction. Surprisingly, loss of Ezh2 did not exert a significant influence on the gene expression profiles in any DC subset analyzed in our study and the global levels of H3K27 methylation remained comparably low in both Ezh2-deficient and wild-type LCs as well as in BMDCs (Gunawan et al., 2015). These data suggest that loss of Ezh2 epigenetic regulation in DCs is likely compensated for by the up-regulation of Ezh1. However, Ezh2 can also methylate a selected number of non-histone substrates (Dasgupta et al., 2015; He et al., 2012; Jung et al., 2013; Lee et al., 2012). We have identified previously that Ezh2 is localized in the cytoplasmic compartment of several immune cells and has potential functions in cytosol (Gunawan et al., 2015; Su et al., 2005). In our current study, we report that cytoplasmic Ezh2-mediated tri-methylation of the integrin adaptor protein Talin1 controls the adhesion dynamics and migratory potential of both human and mouse skin LCs. Our data indicate that Ezh2 is essential for LC trafficking to the sdLNs under both steady-state and inflammatory conditions and therefore plays a pivotal role in cutaneous tolerance induction. In the absence of Ezh2, LCs were frequently found to be trapped on the basement membrane and displayed atypical turnover of adhesion structures, leading to increased cell spreading and defective integrin-dependent migration on laminin-coated surfaces. Accordingly, *CD11c-cre; Ezh2$^{f/f}$* mice displayed progressive accumulation of LCs in the epidermis with increasing age, which could not be explained by Ezh2 effects on basal proliferation or apoptotic rates. It is therefore likely that LC accumulation over time is due to the impaired steady-state emigration of Ezh2-deficient cells from the skin.

Maintaining constant DC numbers in peripheral tissues and lymphoid organs is critical to ensuring a balance between protective and pathological immune activation, but it remains poorly understood how this process is regulated *in vivo*. A previous study suggested that loss of DC from the tissues triggers a feedback mechanism that stimulates recruitment and differentiation of pre-cDCs (Hochweller et al., 2009). However, we observed that Ezh2-deficient LCs continued to replenish themselves in steady state even when cell numbers exceeded normal population numbers. Since LCs' down-regulation of E-cadherin and migration toward basement membrane were not affected by Ezh2 deficiency, it is possible that the stalled Ezh2-deficient LCs on basement membrane is sufficient to stimulate LCs or their precursors to proliferate/differentiate and occupy the new niche. Proximity to keratinocytes may therefore be an important influence on sensing and control of LC numbers in the epidermis. A role for Ezh2 in the homeostatic regulation of LC numbers remains possible, whereas steady-state DC numbers in other organs such as the spleen and thymus, where a physical barrier like basement membrane is not present, are unaffected by Ezh2 deficiency (Gunawan et al., 2015) (data not shown). We therefore propose that the observed age-dependent accumulation of Ezh2-deficient LCs in the epidermis is due to reduced steady-state egress from the skin.

LCs are thought to depend on integrin-based adhesions to migrate and must cross the basement membrane to reach sdLNs, whereas dDCs migrate via actomyosin contractions and can directly access the lymphatic vessels, which contain little or no basement membrane (Lammermann et al., 2008). As such, only the migration of Ezh2-deficient epidermal LCs, but not dDCs, to sdLNs is impaired. In line with these data, control and *CD11c-cre; Ezh2$^{f/f}$* mice were observed to respond equally to DNFB-mediated CHS upon

tolerization with high-dose DNTB. This also suggests that pro-inflammatory gene expression in DCs is not released from repression by loss of the transcriptional silencer Ezh2, unlike what has been reported in the case of other Ezh2 inhibitor-treated leukocytes (McCabe et al., 2012). Although this redundancy of LCs with dDCs during cutaneous tolerization is consistent with earlier reports (Honda et al., 2010; Noordegraaf et al., 2010), studies by others have yielded seemly conflicting observations (Bobr et al., 2010; Kaplan et al., 2005). Their studies suggest a non-redundant role of LCs in tolerance induction by depleting LCs using human diphtheria toxin receptor/diphtheria toxin system. In our experimental model, the Ezh2-deficient LCs could not migrate and deliver allergen/tolerogen to sdLNs and the dDCs were also Ezh2-deficient with potentially altered functions. When we treated the animals with high-dose DNTB, we promoted, as reported (Noordegraaf et al., 2010), the dissemination of hapten into the dermis and the migration of a specific subset of dDCs (Langerin$^-$ or CD11b$^+$) in both control and *CD11c-cre; Ezh2$^{f/f}$* mice. However, Ezh2-deficient dDCs were able to rescue tolerance induction in the absence of LCs. Hence, apart from regulating the migration of LCs, Ezh2 plays a role in controlling the tolerogenic properties of dDCs as well.

A previous *in vivo* DC-targeting study suggested the superior ability of Langerin$^+$ dDCs to induce Treg conversion (Idoyaga et al., 2013), whereas in our system we did not observe these cells to migrate to the sdLNs in response to high-dose DNTB. Given that the Langerin$^+$ DC population of the dermis is relatively small compared with the Langerin$^-$ DC population, their influence on tolerance induction via hapten exposure may be limited. Similarly, a previous study utilizing the same tolerization and sensitization regimen observed migration of both LCs and Langerin$^-$ DCs, but not Langerin$^+$ DCs, to the sdLNs in response to DNTB application. However, they reported that only LCs are capable of inducing CD8$^+$ T cell anergy and Foxp3$^+$ Tregs activation to promote cutaneous tolerance (Gomez de Aguero et al., 2012). Here, we observed that increased number of migratory Ezh2-deficient Langerin$^-$ dDCs was correlated with restored tolerance in *CD11c-cre; Ezh2$^{f/f}$* mice upon treatment with high-dose DNTB, because they possess higher ALDH activity and expression than wild-type counterparts, which catalyzes retinoic acid synthesis and thereby mediates Treg differentiation (Guilliams et al., 2010). Even though the overall gene expression profile of DCs was unaffected by Ezh2 deficiency, *Aldh* is one of the few genes found to be up-regulated in Ezh2-deficient DCs. It is likely that the increased expression of ALDH enhances the tolerogenic capacity of Ezh2-deficient Langerin$^-$ dDCs and thereby enables cutaneous tolerance in the absence of LCs upon exposure to high-dose DNTB. Our findings therefore suggest that modulation of the Ezh2 level in Langerin$^-$ dDCs may serve as an approach for the therapeutic induction of cutaneous tolerance. However, further study will be required to fully elucidate the tolerizing properties of these cutaneous DC subsets before effective treatment strategies can be designed to enhance host protection against skin allergy and autoimmune diseases.

Taken together, our data establish a critical role for Ezh2 in the control of LC transmigration across the basement membrane and the regulation of ALDH activity in Langerin$^-$ dDCs, thereby promoting the induction of skin tolerance toward innocuous haptens. Our findings that Ezh2 regulates LC- and DC-mediated immune responses may also extend to other inflammatory skin disorders in which LC migration and dDC tolerogenic potential have been identified as critical determinants of disease outcome, such as psoriasis and *Candida albicans* infection (Cumberbatch et al., 2006; Igyarto et al., 2011). To further support the discovery made in our animal studies, we observed in publicly available microarray expression database a trend of reduced Ezh2 expression in skin sample derived from patients with dermatitis and psoriasis compared with healthy controls (De Benedetto et al., 2011), highlighting the potential correlation between Ezh2 expression and cutaneous health. Hence, novel strategies that modulate the nuclear and cytosolic functions of Ezh2 in DCs may represent effective therapeutic approaches for various types of cutaneous diseases.

Limitations of Study

In this study, we demonstrated the association between epigenetic de-repression of *Aldh* and enhanced tolerogenicity of Ezh2-deficient dDCs. However, we did not directly address the contribution of high ALDH activity in Ezh2-deficient Langerin$^-$ dDCs to the rescue of tolerance in *CD11c-cre; Ezh2$^{f/f}$* mice upon treatment with a high dosage of haptens. This will require the generation of additional mouse model to conditionally inactivate all *Aldh* loci in Ezh2-deficient dDCs of chimeric mice with ALDH-expressing Ezh2-deficient LCs. Such genetic tool is currently not available, and chemical inhibition or short hairpin RNA-mediated knockdown is likely to affect both LC and dDC at the same time in any *in vivo* setting. Nevertheless, since ALDH-associated tolerogenic capacity of Langerin$^-$ (CD11b$^+$) dDCs in promoting

Treg differentiation has been demonstrated in previous study (Guilliams et al., 2010) and the Langerin$^-$ (CD11b$^+$) dDCs were the only Ezh2-deficient skin DC population that migrated into sdLN upon high-dose DNTB treatment, Ezh2-deficient Langerin$^-$ dDCs are very likely to contribute to the rescued tolerance induction in the absence of LCs.

METHODS

All methods can be found in the accompanying Transparent Methods supplemental file.

DATA AND SOFTWARE AVAILABILITY

The accession number for the RNA-sequencing data reported in this paper is: GSE122206.

SUPPLEMENTAL INFORMATION

Supplemental Information includes Transparent Methods and five figures and can be found with this article online at https://doi.org/10.1016/j.isci.2018.11.019.

ACKNOWLEDGMENTS

We thank H.Y. Lim and V. Angeli for their suggestions on skin imaging, S. Kasuya for technical assistance on the human skin experiments, and C. Ruedl for critical reading of the manuscript. The study benefitted from the data assembled by the ImmGen consortium. Dr. Neil McCarthy of Insight Editing London critically reviewed the manuscript. This work was mainly supported by the Ministry of Education Singapore (AcRF-Tier1-RG40/13, RG36/17, and MOE2013-T2-2-038) and Ministry of Health, National Medical Research Council (NMRC-CBRG/0057/201) to I.-h.S., and was also funded by Grants-in-Aid for Challenging Exploratory Research (16K15259), Scientific Research B (16H05177) from the Japan Society for the Promotion of Science, Grant-in-Aid for Scientific Research on Innovative Area (17H05798) from the MEXT, Toyoaki Scholarship Foundation, and Kobayashi International Scholarship Foundation to S.Y. These funding bodies played no role in the study design, data collection or analysis, the decision to publish, or preparation of the manuscript.

AUTHOR CONTRIBUTIONS

J.T.L. designed and conducted all the experiments, interpreted data, and wrote the manuscript. B.J., F.G., and M.P. helped with LC sorting and RNA sequencing. M.G. identified migration defect in LCs. T.J.F.L. and M.B. analyzed aldehyde dehydrogenase activity in DCs. K.I. and T.M. performed human skin experiments. T.T. provided human clinical samples. A.M. analyzed human skin data. L.G.N. performed intravital imaging. S.Y. designed and performed human experiments, analyzed data, and contributed to manuscript preparation. K.-P.L. was involved in critical discussion and laboratory support. I.-h.S. was involved in data interpretation and manuscript preparation.

DECLARATION OF INTERESTS

The authors declare no competing interests.

Received: August 31, 2018
Revised: October 24, 2018
Accepted: November 9, 2018
Published: December 21, 2018

REFERENCES

Bobr, A., Olvera-Gomez, I., Igyarto, B.Z., Haley, K.M., Hogquist, K.A., and Kaplan, D.H. (2010). Acute ablation of Langerhans cells enhances skin immune responses. J. Immunol. *185*, 4724–4728.

Cao, Q., Yu, J., Dhanasekaran, S.M., Kim, J.H., Mani, R.S., Tomlins, S.A., Mehra, R., Laxman, B., Cao, X., Yu, J., et al. (2008). Repression of E-cadherin by the polycomb group protein EZH2 in cancer. Oncogene *27*, 7274–7284.

Cao, R., Wang, L., Wang, H., Xia, L., Erdjument-Bromage, H., Tempst, P., Jones, R.S., and Zhang, Y. (2002). Role of histone H3 lysine 27 methylation in Polycomb-group silencing. Science *298*, 1039–1043.

Cumberbatch, M., Singh, M., Dearman, R.J., Young, H.S., Kimber, I., and Griffiths, C.E. (2006). Impaired Langerhans cell migration in psoriasis. J. Exp. Med. *203*, 953–960.

Czermin, B., Melfi, R., McCabe, D., Seitz, V., Imhof, A., and Pirrotta, V. (2002). Drosophila enhancer of Zeste/ESC complexes have a histone H3 methyltransferase activity that marks chromosomal Polycomb sites. Cell *111*, 185–196.

Dasgupta, M., Dermawan, J.K., Willard, B., and Stark, G.R. (2015). STAT3-driven transcription depends upon the dimethylation of K49 by EZH2. Proc. Natl. Acad. Sci. U S A *112*, 3985–3990.

De Benedetto, A., Rafaels, N.M., McGirt, L.Y., Ivanov, A.I., Georas, S.N., Cheadle, C., Berger, A.E., Zhang, K., Vidyasagar, S., Yoshida, T., et al. (2011). Tight junction defects in patients with atopic dermatitis. J. Allergy Clin. Immunol. *127*, 773–786.e1–7.

Franco, S.J., Rodgers, M.A., Perrin, B.J., Han, J., Bennin, D.A., Critchley, D.R., and Huttenlocher, A. (2004). Calpain-mediated proteolysis of talin regulates adhesion dynamics. Nat. Cell Biol. *6*, 977–983.

Fukunaga, A., Khaskhely, N.M., Sreevidya, C.S., Byrne, S.N., and Ullrich, S.E. (2008). Dermal dendritic cells, and not Langerhans cells, play an essential role in inducing an immune response. J. Immunol. *180*, 3057–3064.

Gomez de Aguero, M., Vocanson, M., Hacini-Rachinel, F., Taillardet, M., Sparwasser, T., Kissenpfennig, A., Malissen, B., Kaiserlian, D., and Dubois, B. (2012). Langerhans cells protect from allergic contact dermatitis in mice by tolerizing CD8(+) T cells and activating Foxp3(+) regulatory T cells. J. Clin. Invest. *122*, 1700–1711.

Guilliams, M., Crozat, K., Henri, S., Tamoutounour, S., Grenot, P., Devilard, E., de Bovis, B., Alexopoulou, L., Dalod, M., and Malissen, B. (2010). Skin-draining lymph nodes contain dermis-derived CD103(-) dendritic cells that constitutively produce retinoic acid and induce Foxp3(+) regulatory T cells. Blood *115*, 1958–1968.

Gunawan, M., Venkatesan, N., Loh, J.T., Wong, J.F., Berger, H., Neo, W.H., Li, L.Y., La Win, M.K., Yau, Y.H., Guo, T., et al. (2015). The methyltransferase Ezh2 controls cell adhesion and migration through direct methylation of the extranuclear regulatory protein talin. Nat. Immunol. *16*, 505–516.

Hacker, C., Kirsch, R.D., Ju, X.S., Hieronymus, T., Gust, T.C., Kuhl, C., Jorgas, T., Kurz, S.M., Rose-John, S., Yokota, Y., et al. (2003). Transcriptional profiling identifies Id2 function in dendritic cell development. Nat. Immunol. *4*, 380–386.

He, A., Shen, X., Ma, Q., Cao, J., von Gise, A., Zhou, P., Wang, G., Marquez, V.E., Orkin, S.H., and Pu, W.T. (2012). PRC2 directly methylates GATA4 and represses its transcriptional activity. Genes Dev. *26*, 37–42.

Hochweller, K., Miloud, T., Striegler, J., Naik, S., Hammerling, G.J., and Garbi, N. (2009). Homeostasis of dendritic cells in lymphoid organs is controlled by regulation of their precursors via a feedback loop. Blood *114*, 4411–4421.

Hoeffel, G., Wang, Y., Greter, M., See, P., Teo, P., Malleret, B., Leboeuf, M., Low, D., Oller, G., Almeida, F., et al. (2012). Adult Langerhans cells derive predominantly from embryonic fetal liver monocytes with a minor contribution of yolk sac-derived macrophages. J. Exp. Med. *209*, 1167–1181.

Honda, T., Nakajima, S., Egawa, G., Ogasawara, K., Malissen, B., Miyachi, Y., and Kabashima, K. (2010). Compensatory role of Langerhans cells and langerin-positive dermal dendritic cells in the sensitization phase of murine contact hypersensitivity. J. Allergy Clin. Immunol. *125*, 1154–1156.e2.

Idoyaga, J., Fiorese, C., Zbytnuik, L., Lubkin, A., Miller, J., Malissen, B., Mucida, D., Merad, M., and Steinman, R.M. (2013). Specialized role of migratory dendritic cells in peripheral tolerance induction. J. Allergy Clin. Immunol. *123*, 844–854.

Igyarto, B.Z., Haley, K., Ortner, D., Bobr, A., Gerami-Nejad, M., Edelson, B.T., Zurawski, S.M., Malissen, B., Zurawski, G., Berman, J., et al. (2011). Skin-resident murine dendritic cell subsets promote distinct and opposing antigen-specific T helper cell responses. Immunity *35*, 260–272.

Igyarto, B.Z., Jenison, M.C., Dudda, J.C., Roers, A., Muller, W., Koni, P.A., Campbell, D.J., Shlomchik, M.J., and Kaplan, D.H. (2009). Langerhans cells suppress contact hypersensitivity responses via cognate CD4 interaction and Langerhans cell-derived IL-10. J. Immunol. *183*, 5085–5093.

Jin, J., Xie, X., Xiao, Y., Hu, H., Zou, Q., Cheng, X., and Sun, S.C. (2016). Epigenetic regulation of the expression of Il12 and Il23 and autoimmune inflammation by the deubiquitinase Trabid. Nat. Immunol. *17*, 259–268.

Jung, H.Y., Jun, S., Lee, M., Kim, H.C., Wang, X., Ji, H., McCrea, P.D., and Park, J.I. (2013). PAF and EZH2 induce Wnt/beta-catenin signaling hyperactivation. Mol. Cell *52*, 193–205.

Kaplan, D.H., Jenison, M.C., Saeland, S., Shlomchik, W.D., and Shlomchik, M.J. (2005). Epidermal langerhans cell-deficient mice develop enhanced contact hypersensitivity. Immunity *23*, 611–620.

Kissenpfennig, A., Henri, S., Dubois, B., Laplace-Builhe, C., Perrin, P., Romani, N., Tripp, C.H., Douillard, P., Leserman, L., Kaiserlian, D., et al. (2005). Dynamics and function of Langerhans cells in vivo: dermal dendritic cells colonize lymph node areas distinct from slower migrating Langerhans cells. Immunity *22*, 643–654.

Koyanagi, M., Baguet, A., Martens, J., Margueron, R., Jenuwein, T., and Bix, M. (2005). EZH2 and histone 3 trimethyl lysine 27 associated with Il4 and Il13 gene silencing in Th1 cells. J. Biol. Chem. *280*, 31470–31477.

Kruidenier, L., Chung, C.W., Cheng, Z., Liddle, J., Che, K., Joberty, G., Bantscheff, M., Bountra, C., Bridges, A., Diallo, H., et al. (2012). A selective jumonji H3K27 demethylase inhibitor modulates the proinflammatory macrophage response. Nature *488*, 404–408.

LaMere, S.A., Thompson, R.C., Komori, H.K., Mark, A., and Salomon, D.R. (2016). Promoter H3K4 methylation dynamically reinforces activation-induced pathways in human CD4 T cells. Genes Immun. *17*, 283–297.

Lammermann, T., Bader, B.L., Monkley, S.J., Worbs, T., Wedlich-Soldner, R., Hirsch, K., Keller, M., Forster, R., Critchley, D.R., Fassler, R., et al. (2008). Rapid leukocyte migration by integrin-independent flowing and squeezing. Nature *453*, 51–55.

Lee, J.M., Lee, J.S., Kim, H., Kim, K., Park, H., Kim, J.Y., Lee, S.H., Kim, I.S., Kim, J., Lee, M., et al. (2012). EZH2 generates a methyl degron that is recognized by the DCAF1/DDB1/CUL4 E3 ubiquitin ligase complex. Mol. Cell *48*, 572–586.

Loh, J.T., and Su, I.H. (2016). Post-translational modification-regulated leukocyte adhesion and migration. Oncotarget *7*, 37347–37360.

Margueron, R., Li, G., Sarma, K., Blais, A., Zavadil, J., Woodcock, C.L., Dynlacht, B.D., and Reinberg, D. (2008). Ezh1 and Ezh2 maintain repressive chromatin through different mechanisms. Mol. Cell *32*, 503–518.

McCabe, M.T., Ott, H.M., Ganji, G., Korenchuk, S., Thompson, C., Van Aller, G.S., Liu, Y., Graves, A.P., Della Pietra, A., 3rd, Diaz, E., et al. (2012). EZH2 inhibition as a therapeutic strategy for lymphoma with EZH2-activating mutations. Nature *492*, 108–112.

Medzhitov, R., and Horng, T. (2009). Transcriptional control of the inflammatory response. Nat. Rev. Immunol. *9*, 692–703.

Merad, M., Manz, M.G., Karsunky, H., Wagers, A., Peters, W., Charo, I., Weissman, I.L., Cyster, J.G., and Engleman, E.G. (2002). Langerhans cells renew in the skin throughout life under steady-state conditions. Nat. Immunol. *3*, 1135–1141.

Natsuaki, Y., Egawa, G., Nakamizo, S., Ono, S., Hanakawa, S., Okada, T., Kusuba, N., Otsuka, A., Kitoh, A., Honda, T., et al. (2014). Perivascular leukocyte clusters are essential for efficient activation of effector T cells in the skin. Nat. Immunol. *15*, 1064–1069.

Noordegraaf, M., Flacher, V., Stoitzner, P., and Clausen, B.E. (2010). Functional redundancy of Langerhans cells and Langerin+ dermal dendritic cells in contact hypersensitivity. J. Invest. Dermatol. *130*, 2752–2759.

Price, A.A., Cumberbatch, M., Kimber, I., and Ager, A. (1997). Alpha 6 integrins are required for Langerhans cell migration from the epidermis. J. Exp. Med. *186*, 1725–1735.

Sere, K., Baek, J.H., Ober-Blobaum, J., Muller-Newen, G., Tacke, F., Yokota, Y., Zenke, M., and Hieronymus, T. (2012). Two distinct types of Langerhans cells populate the skin during steady state and inflammation. Immunity *37*, 905–916.

Shen, X., Liu, Y., Hsu, Y.J., Fujiwara, Y., Kim, J., Mao, X., Yuan, G.C., and Orkin, S.H. (2008). EZH1 mediates methylation on histone H3 lysine 27 and complements EZH2 in maintaining stem cell identity and executing pluripotency. Mol. Cell *32*, 491–502.

Shin, Y.J., and Kim, J.H. (2012). The role of EZH2 in the regulation of the activity of matrix metalloproteinases in prostate cancer cells. PLoS One *7*, e30393.

Stenn, K.S., Link, R., Moellmann, G., Madri, J., and Kuklinska, E. (1989). Dispase, a neutral protease from *Bacillus polymyxa*, is a powerful fibronectinase and type IV Collagenase. J. Invest. Dermatol. *93*, 287–290.

Stratis, A., Pasparakis, M., Rupec, R.A., Markur, D., Hartmann, K., Scharffetter-Kochanek, K., Peters, T., van Rooijen, N., Krieg, T., and Haase, I. (2006). Pathogenic role for skin macrophages in a mouse model of keratinocyte-induced psoriasis-like skin inflammation. J. Clin. Invest. *116*, 2094–2104.

Su, I.H., Basavaraj, A., Krutchinsky, A.N., Hobert, O., Ullrich, A., Chait, B.T., and Tarakhovsky, A. (2003). Ezh2 controls B cell development through

histone H3 methylation and Igh rearrangement. Nat. Immunol. *4*, 124–131.

Su, I.H., Dobenecker, M.W., Dickinson, E., Oser, M., Basavaraj, A., Marqueron, R., Viale, A., Reinberg, D., Wulfing, C., and Tarakhovsky, A. (2005). Polycomb group protein ezh2 controls actin polymerization and cell signaling. Cell *121*, 425–436.

Tang, A., Amagai, M., Granger, L.G., Stanley, J.R., and Udey, M.C. (1993). Adhesion of epidermal Langerhans cells to keratinocytes mediated by E-cadherin. Nature *361*, 82–85.

van der Aar, A.M., Picavet, D.I., Muller, F.J., de Boer, L., van Capel, T.M., Zaat, S.A., Bos, J.D., Janssen, H., George, T.C., Kapsenberg, M.L., et al. (2013). Langerhans cells favor skin flora tolerance through limited presentation of bacterial antigens and induction of regulatory T cells. J. Invest. Dermatol. *133*, 1240–1249.

Venkatesan, N., Wong, J.F., Tan, K.P., Chung, H.H., Yau, Y.H., Cukuroglu, E., Allahverdi, A., Nordenskiold, L., Goke, J., Geifman-Shochat, S., et al. (2018). EZH2 promotes neoplastic transformation through VAV interaction-dependent extranuclear mechanisms. Oncogene *37*, 461–477.

Villablanca, E.J., and Mora, J.R. (2008). A two-step model for Langerhans cell migration to skin-draining LN. Eur. J. Immunol. *38*, 2975–2980.

Xu, C., Hou, Z., Zhan, P., Zhao, W., Chang, C., Zou, J., Hu, H., Zhang, Y., Yao, X., Yu, L., et al. (2013). EZH2 regulates cancer cell migration through repressing TIMP-3 in non-small cell lung cancer. Med. Oncol. *30*, 713.

Yurchenco, P.D. (2011). Basement membranes: cell scaffoldings and signaling platforms. Cold Spring Harb. Perspect. Biol. *3*, https://doi.org/10.1101/cshperspect.a004911.

ISCI, Volume *10*

Supplemental Information

Ezh2 Controls Skin Tolerance through Distinct Mechanisms in Different Subsets of Skin Dendritic Cells

Jia Tong Loh, Thomas Jun Feng Lim, Kyoko Ikumi, Takuma Matoba, Baptiste Janela, Merry Gunawan, Tatsuya Toyama, Maegan Bunjamin, Lai Guan Ng, Michael Poidinger, Akimichi Morita, Florent Ginhoux, Sayuri Yamazaki, Kong-Peng Lam, and I-hsin Su

Supplemental Figures

- Figure S1: Enhanced cytotoxic T cell responses during elicitation phase of CHS in DNTB-tolerized *CD11c-cre; Ezh2$^{f/f}$* mice. Related to Figure 1.
- Figure S2: Comparable gene expression profiles between Ezh2$^{f/f}$ and Ezh2$^{\Delta/\Delta}$ LCs. Related to Figure 1.
- Figure S3: Age-dependent accumulation of Ezh2-deficient LCs due to impaired steady state migration. Related to Figure 2.
- Figure S4: Ezh2 deficiency does not affect expression of adhesion-related molecules and MMP activities of LCs. Related to Figures 2-4.
- Figure S5: Ezh2-mediated Talin1 methylation at K2454 promotes LC migration. Related to Figure 5.

Transparent Methods

Supplemental References

Supplemental Figures

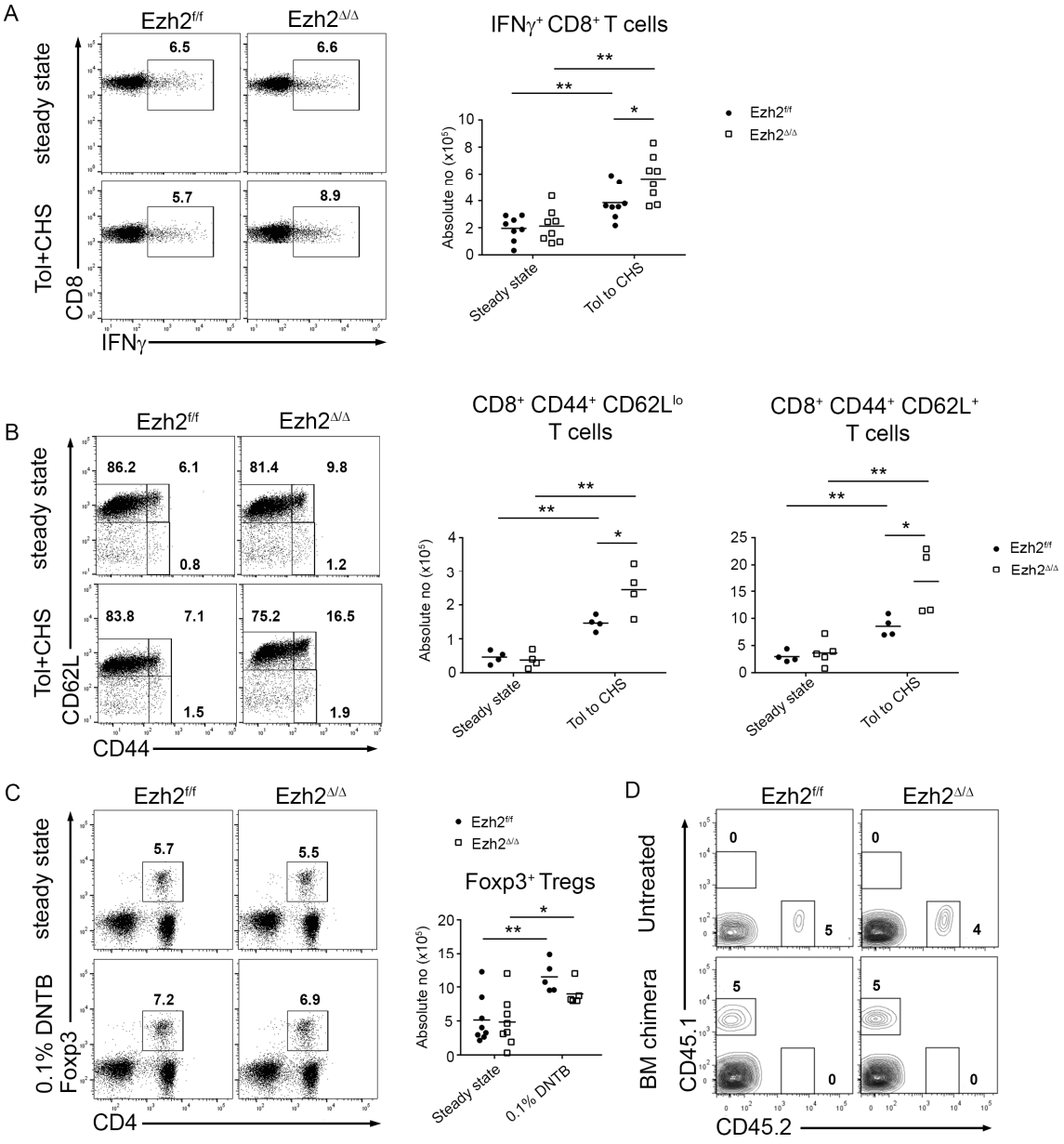

Figure S1: Enhanced cytotoxic T cell responses during elicitation phase of CHS in DNTB-tolerized *CD11c-cre; Ezh2$^{f/f}$* mice. Related to Figure 1.

(A and B) Mice were tolerized (Tol) on shaved abdomen skin with 0.1% DNTB before sensitization with 0.5% DNFB on shaved back skin 7 days later. SdLNs were harvested after 5 days. (A) Flow cytometric analyses of IFNγ-producing CD8$^+$ T cells in the sdLNs during steady state and following tolerization to CHS. Dot plots were pregated on singlet, live, CD3ε$^+$, CD8$^+$, CD4$^-$ cells. Scatter plot indicates absolute numbers of IFNγ-producing CD8$^+$ T cells. Data is based on 4 independent experiments (n=8). From left to right, **P*=0.03. ***P*=0.004, 0.0003. (two-tailed Student's *t*-test).

(B) Flow cytometric analyses of $CD8^+$ T cells activation status in the sdLNs during steady state and following tolerization to CHS. Dot plots were pregated on singlet, live, $CD3\varepsilon^+$, $CD8^+$, $CD4^-$ cells. Scatter plot indicates absolute numbers of $CD44^+$ $CD62L^{lo}$ effector and $CD44^+$ $CD62L^+$ central-memory $CD8^+$ T cells. Data is based on 3 independent experiments (n=4). From left to right, **P*=0.03, 0.04. ***P*=0.0005, 0.001, 0.002, 0.003. (two-tailed Student's *t*-test).

(C) Flow cytometric analyses of $CD4^+$ $Foxp3^+$ T regulatory cells in sdLNs during steady state and 5 days following tolerization with 0.1% DNTB. Dot plots were pre-gated on singlet, live cells, $CD3\varepsilon^+$ cells. Data is based on 3 independent experiments (n>5). From left to right, **P*=0.03. ***P*=0.004. (two-tailed Student's *t*-test).

(D) Flow cytometric analyses of CD45.1 vs CD45.2 cells in blood harvested from untreated control recipient mice or bone marrow (BM) chimeras 8 weeks after irradiation and transplantation. *Ezh2*$^{f/f}$ and *CD11c-cre; Ezh2*$^{f/f}$ mice (CD45.2) were used as recipients. CD45.1 wild type mice were used as donors. Contour plots were pre-gated on singlet cells.

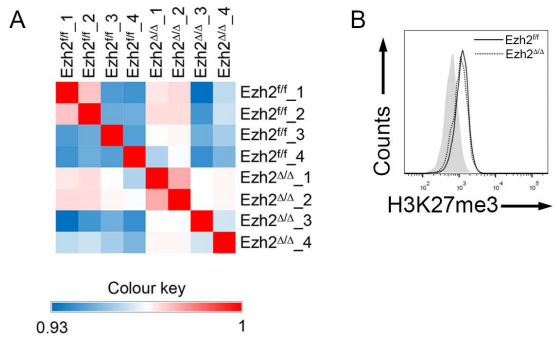

Figure S2: Comparable gene expression profiles between Ezh2$^{f/f}$ and Ezh2$^{\Delta/\Delta}$ LCs. Related to Figure 1.

(A) Heatmap of Pearson correlation coefficient scores derived from RNA-seq analysis of sorted epidermal control (Ezh2$^{f/f}$) and Ezh2-deficient (Ezh2$^{\Delta/\Delta}$) LCs (n=4).

(B) Total H3K27me3 levels in epidermal LCs isolated from freshly excised mouse ears were analysed by intracellular staining and flow cytometry. Histograms were pregated on singlet, live, CD11c^{+} MHC II^{+} EpCAM^{+} CD103^{-} cells. Solid line represents control LCs, and dotted line represents Ezh2-deficient LCs. Filled histogram represents isotype control. Data shown is representative of 3 independent experiments (n=3).

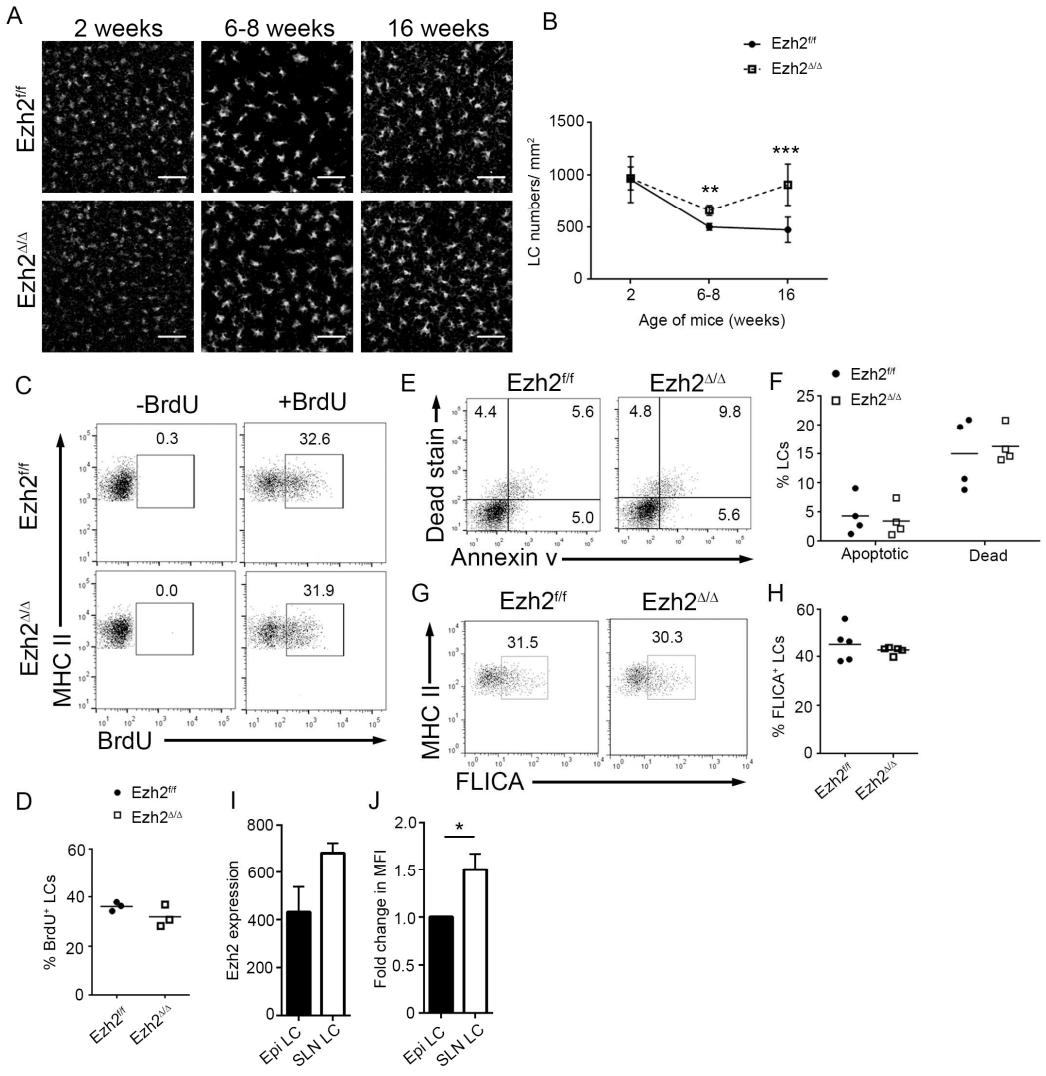

Figure S3: Age-dependent accumulation of Ezh2-deficient LCs due to impaired steady state migration. Related to Figure 2.

(A) Epidermal sheets isolated from mice of different age groups (as indicated) were stained with anti-MHC II antibody. Images shown are representative of at least 2 independent experiments (n=3-4, ≥6 fields per group). Scale bars, 50 μm.

(B) Graph indicates LC numbers/mm^2 (mean±SD). Data is based on at least 2 independent experiments (n=3-4, ≥6 fields per group). ***P*=0.0007. ****P*=8x10^{-5}. (two-tailed Student's *t*-test).

(C) Mice were injected intraperitoneally with BrdU and subsequently administered with BrdU-supplemented drinking water for 7 days. MHC II$^+$ CD11c$^+$ EpCAM$^+$ CD103$^-$ live epidermal LCs were analysed for their incorporation of BrdU by flow cytometry.

(D) Scatter plot indicates the percentages of BrdU-positive LCs (n=3).

(E) The frequency of apoptotic LCs was analysed by Annexin V staining. Dead LCs are identified by their positive staining for the viability dye.

(F) Scatter plot indicates the percentages of apoptotic (lower right quadrant) and dead (upper quadrants) LCs. Data shown is representative of 3 independent experiments (n=4).

(G) Apoptotic LCs were determined by labelling with FLICA.

(H) Scatter plot indicates percentage of apoptotic FLICA-positive LCs. (n=5).

(I) Expression of *Ezh2* mRNA by epidermis-resident LCs and sdLN migratory LCs (data from Immunological Genome Project Consortium).

(J) Total Ezh2 levels in epidermis-resident LCs and sdLN migratory LCs were analysed by intracellular staining and flow cytometry. Bar graphs indicate fold change in MFI of Ezh2 in sdLN migratory LCs relative to epidermis-resident LCs. (n=3). **P*=0.02. (two-tailed Student's *t*-test).

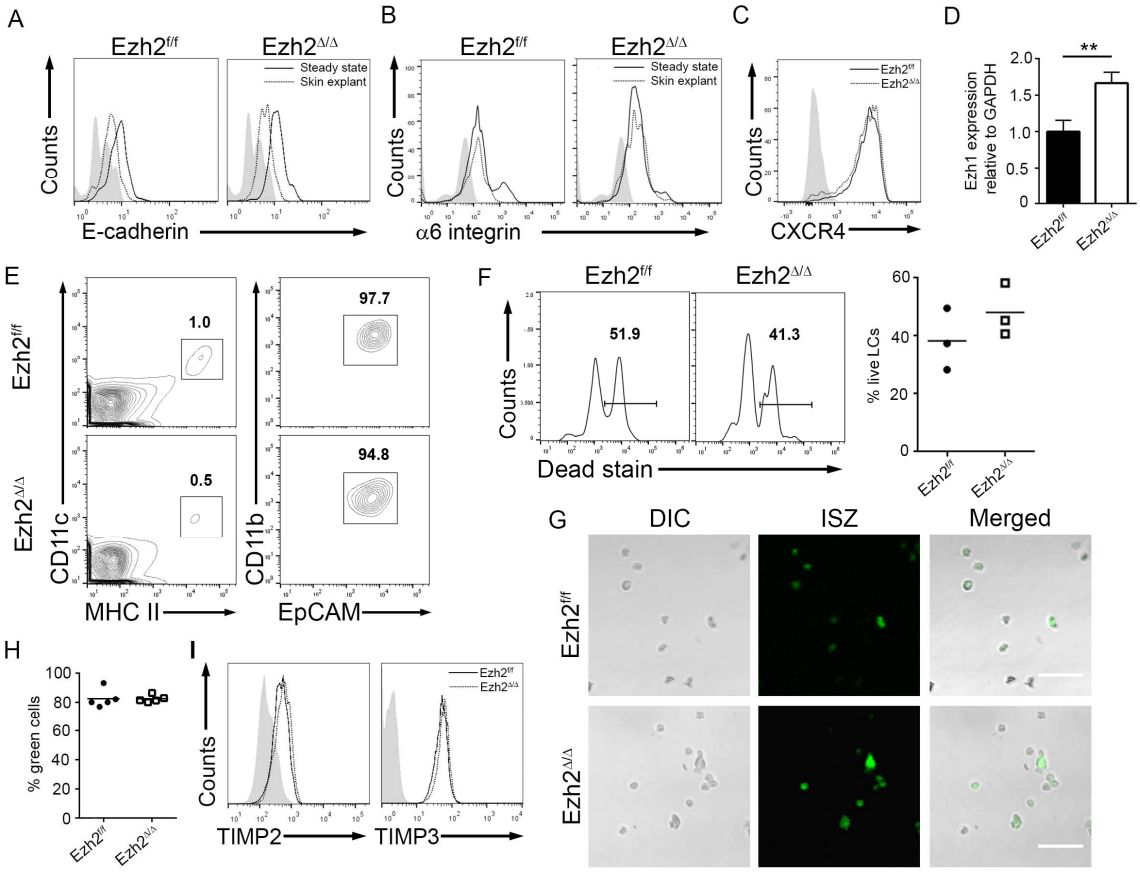

Figure S4: Ezh2 deficiency does not affect expression of adhesion-related molecules and MMP activities of LCs. Related to Figures 2-4.

(A) E-cadherin and (B) integrin α6 expression on epidermal LCs. Solid line represents LCs at steady state, and dotted line represents LCs which have been activated by culture. Filled histogram represents isotype control. Data shown is representative of 3 independent experiments (n=3).

(C) CXCR4 expression on steady state epidermal LCs. Solid line represents control LCs, and dotted line represents Ezh2-deficient LCs. Filled histogram represents isotype control. Data shown is representative of 3 independent experiments (n=3).

(D) *Ezh1* expression in control and Ezh2-deficient mature BMDCs. Gene expression was normalized against *GAPDH*. ***P*=0.006. (two-tailed Student's *t*-test).

(E and F) Emigration of Ezh2-deficient LCs following epidermal sheet culture in the absence of basement membrane. (E) Epidermis was isolated by dispase digestion, and cultured for 4 hours before flow cytometric analyses. Contour plots were pre-gated on singlet, live cells. $CD11c^{+}$ MHC II^{+} DCs were further analysed for $CD103^{-}$ $EpCAM^{+}$ LCs. Data shown is representative of 2 independent experiments (n=3). (F) Cells were retrieved from the medium 4 hours following epidermal sheet

culture and analysed by flow cytometry. Percentages of dead LCs were indicated. Data shown is representative of 2 independent experiments (n=3). Scatter plot indicates percentages of live LCs retrieved from the culture medium. Data is based on 2 independent experiments (n=3).

(G and H) *In situ* zymography (ISZ) of LCs. Purified epidermal LCs were incubated with DQ-gelatin for 4 hours. Green fluorescent staining revealed MMP proteolytic activity in LCs (n=3). Scale bars, 50 μm. Scatter plot indicates percentage of LCs with active MMPs (n=3; 5 fields per group), (two-tailed Student's *t*-test).

(I) Expression of TIMP2 and TIMP3 on steady state epidermal LCs. Solid line represents control LCs, and dotted line represents Ezh2-deficient LCs. Filled histogram represents isotype control. Data shown is representative of 3 independent experiments (n=3).

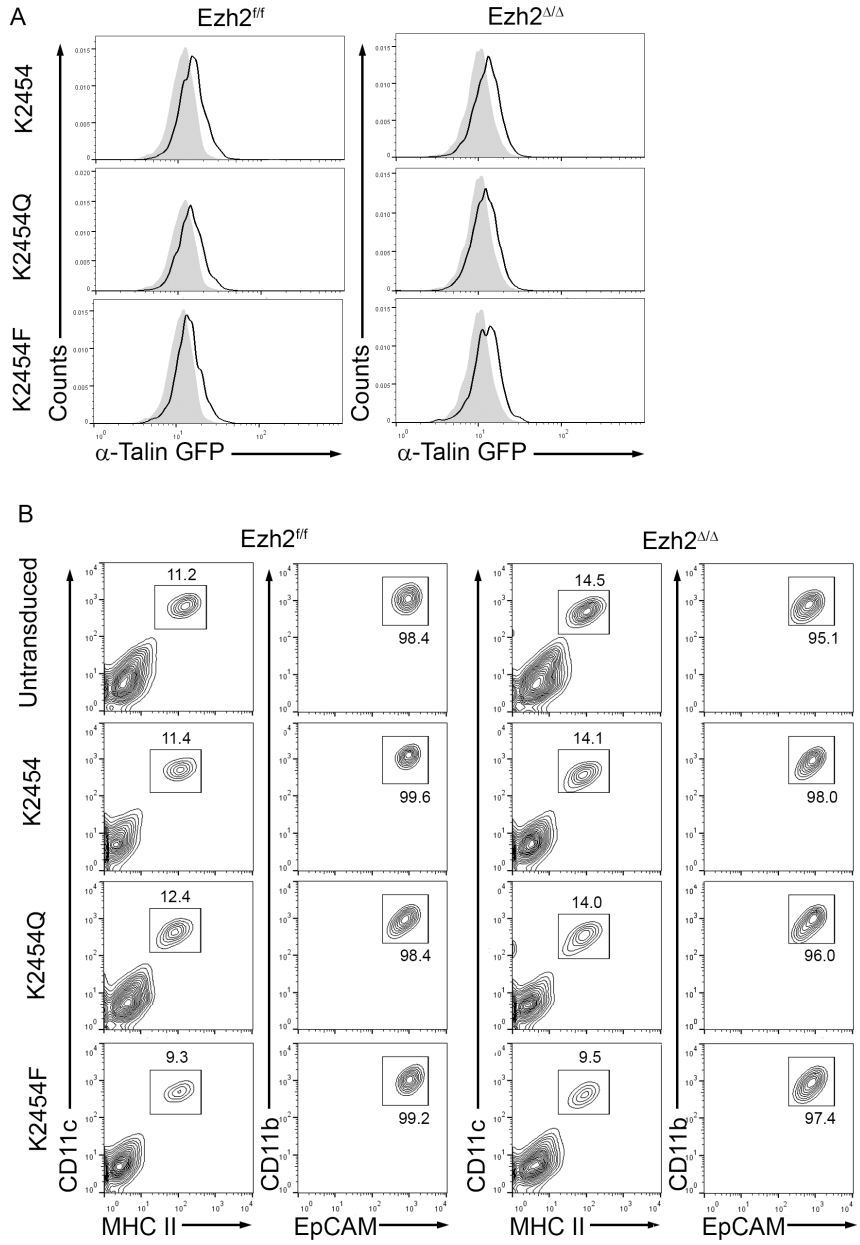

Figure S5: Ezh2-mediated Talin1 methylation at K2454 promotes LC migration. Related to Figure 5.

Mice ears were tape-stripped and infected with retroviral vector carrying different GFP-tagged Talin1 mutants (K2454, K2454Q, K2454F). Epidermal sheets were harvested and analysed by flow cytometry.

(A) Transduction efficiency of GFP-tagged Talin1 mutants were determined by flow cytometry. Histograms were pre-gated on singlet, live, MHC II^+ $CD11c^+$ $EpCAM^+$ $CD11b^+$ cells. Filled histogram represents untransduced control.

(B) Contour plots were pre-gated on singlet, live, $CD45^+$ cells. MHC II^+ $CD11c^+$ DCs in the epidermis were further analysed for $CD11b^+$ $EpCAM^+$ LCs.

Transparent Methods

Mice

CD11c-cre; Ezh2$^{f/f}$ mice, *CD11c-cre; CD11c-YFP; Ezh2$^{f/f}$* mice and *Mx1-cre; Ezh2$^{f/f}$* mice were generated as described (Gunawan et al., 2015). All mice were bred and maintained under specific pathogen-free conditions at the animal facility of the School of Biological Sciences, Nanyang Technological University, Singapore. Mice were used at 6-8 weeks of age unless otherwise stated.

Preparation of skin single cell suspensions

Ears were split into dorsal and ventral halves and floated on Hank's balanced salt solution containing Dispase (Invitrogen) for 45min at 37^{o}C to allow separation of the epidermis from the dermis. For immunofluorescence analysis, the epidermal sheet was then fixed in acetone for 20min at -20^{o}C. For flow cytometric analysis, epidermal and dermal sheets were cut into small pieces and digested in complete RPMI-1640 medium (10% FCS, 2-mercaptoethanol and penicillin-streptomycin) (Gibco-BRL) containing Liberase TM Research Grade (Roche) and DNase I (Roche) for 1.5h at 37^{o}C. Tissue fragments were then homogenized using a 1ml syringe prior to filtration through a 70µm nylon mesh to obtain a homogeneous single cell suspension.

Isolation and culture of BMDCs

BM cells were harvested from *Ezh2$^{f/f}$* and *Mx1-cre; Ezh2$^{f/f}$* mice and cultured in complete RPMI-1640 medium (10% FCS, 2-mercaptoethanol and penicillin-streptomycin) (Gibco-BRL) supplemented with 20ng/ml of GM-CSF and 10ng/ml of IL-4 (Prospec Tany). On day 2 of culture, the cells were gently washed and the medium replaced with fresh complete medium supplemented with 10ng/ml GM-CSF. Cells were cultured for 5 to 6 days. For the generation of mature BMDCs, cells were stimulated overnight with 100ng/ml LPS (Sigma-Aldrich).

Skin explant assay

Split ear halves were cultured in 1.5ml complete RPMI-1640 medium in 24-well tissue culture plates for 18h at 37^{o}C. In some experiments, the epidermal sheet was separated from the dermis prior to culture for 4h duration.

LC migration assay with human skin explants

Human full thickness of skin was eliminated of fat completely by scissors and cut into 7x7 mm pieces. The pieces of skin were floated on RPMI with 5% FCS medium in 24-well plates with the Ezh2 inhibitor, GSK126 (Active Biochemicals, HongKong, China) at a final concentration of 100μM or the control, same concentration of DMSO (Sigma). After 1-3 day of culture, cells migrated into the 24-wells were collected by pipetting and live cells were counted in the presence of trypan blue (Gibco). Collected cells were stained with anti-human CD45-pacific blue, HLA-DR-alexa700, CD1a-alexa488 (Biolegend) and CD11c-PE (BD Pharmingen) antibodies and analysed by an FACS Verse flow cytomter (BD Bioscience). Data was analysed by FlowJo software version 9 (FlowJo LLC., Ashland, OR, USA). Cell numbers of each population were calculated from the frequency and cell numbers.

Flow cytometry

Cell suspensions were surface-labelled with monoclonal antibodies for 10min at 4^{o}C in staining buffer (PBS containing 0.5% BSA and 0.01% sodium azide). For intracellular labelling, the cells were then fixed and permeabilized using the Cytofix/Cytoperm kit (BD) or Foxp3 staining buffer set (eBioscience) according to the manufacturer's protocol before staining for 1h at room temperature. Fixable viability dye (eBioscience) was used to exclude dead cells. Single cell suspensions were acquired using LSRII or LSRFortessa flow-cytometers (BD Biosciences) for subsequent analysis using FlowJo software (Tree Star).

Oxazolone painting

A total 25μl volume of 0.5% oxazolone (Sigma-Aldrich) was dissolved in acetone:olive oil (4:1, v/v) and painted on both the dorsal and ventral sides of mouse ears. The mice were then sacrificed 24h or 48h after sensitization and their ears or skin draining lymph nodes were harvested for further analysis.

BrdU labelling *in vivo*

Mice were administered 1mg BrdU (Sigma-Aldrich) in PBS via intraperitoneal injection and then supplied with fresh drinking water containing 0.8mg/ml BrdU (refreshed daily) for an additional 7 days. Single cell suspensions were prepared as described above and BrdU intracellular staining was performed using the FITC BrdU Flow kit (BD Pharmingen) according to the manufacturer's protocol.

AldeFluor^{TM} staining

Aldehyde dehydrogenase activity in BMDCs was determined using AldeFluor™ kit (Stemcell Technologies) according to the manufacturer's protocol.

Induction of tolerance to CHS

Mice were tolerized by skin painting with a 100µl volume of 0.1/1% DNTB (Lancaster Synthesis) in vehicle consisting of acetone and olive oil (AOO) (4:1, v/v) applied to the shaved abdominal skin. Seven days later, the mice were sensitized by skin painting with a 25µl volume of 0.5% DNFB (Sigma-Aldrich) in AOO onto the shaved back skin. Five days later, mouse organs were harvested for analysis or the mice were further challenged using a 4µl volume of 0.1% DNFB in AOO applied to both dorsal and ventral sides of the ear. Ear swelling was measured using a micrometer (Mitutoyo) by a blinded observer.

Retroviral infection of skin

Mouse ears were subjected to tape-stripping (5 repetitions) before application of retrovirus encoding Talin1 mutants K2454Q or K2454F (or GFP-tagged-Talin1 K2454 control) in the presence of polybrene. The procedure was repeated 24h later. After 4 days, the mice were either sacrificed or subjected to oxazolone skin painting for analysis of LC migration.

Generation of bone marrow chimeras

Bone marrow cells were isolated from the femurs and tibias of donor mice for intravenous injection into sex-matched recipients that had been subjected to lethal irradiation (2x5.5Gy administered 4h apart). Mice were maintained on antibiotic-supplemented water (Neomycin sulfate; Sigma-Aldrich) for 2w thereafter and used in experiments 8w after transplantation.

Skin sectioning

Footpad skin was fixed overnight at 4^{o}C in 2% paraformaldehyde containing 30% sucrose. Fixed skin samples were embedded in OCT compound, sliced into 20µm-thick sections, and stained with anti-laminin (abcam) and AlexaFluor 647-X-AffiniPure Goat Anti-Rabbit IgG (Jackson ImmunoResearch Laboratories, Inc.) before mounting in DAPI-supplemented mounting medium (Ibidi).

Focal adhesion imaging

LCs were allowed to adhere to 8-well culture slides (BD Falcon) that were coated with 10µg/ml Laminin derived from Engelbreth-Holm-Swarm murine sarcoma basement membrane (Sigma-Aldrich). Cells were incubated at 37^{o}C for 2h before removal of non-adherent cells by gentle washing with PBS. Adherent cells were fixed with 2% paraformaldehyde for 15min at room temperature and then permeabilized with 0.5% Triton X-100 for 5min at 4^{o}C. Fixed cells were blocked for 1h using 10% normal donkey serum (Sigma-Aldrich) in PBS containing BSA, sodium azide and 0.5% saponin. The cells were then labelled overnight at 4^{o}C with monoclonal anti-Talin (clone 8d4, Sigma-Aldrich) before staining with Rhodamine Red- or fluorescein isothiocyanate-X-AffiniPure Donkey Anti-Mouse IgG (Jackson ImmunoResearch Laboratories, Inc.) for 1h at room temperature. LCs were identified by staining with biotin I-A/I-E antibody for 30min at 4^{o}C, followed by addition of Streptavidin-AlexaFluor 647 conjugate for 30min at 4^{o}C prior to mounting. Analysis of adhesion structures was conducted using the following criteria: Nascent adhesions<0.2 µm^2, 0.2 µm^2<focal complexes<0.8 µm^2, 0.8 µm^2<focal adhesions<19 µm^2.

Cell motility assay

LCs were allowed to adhere to 8-well culture slides (BD Falcon) that were coated with 10µg/ml Laminin derived from Engelbreth-Holm-Swarm murine sarcoma basement membrane (Sigma-Aldrich). Non-adherent cells were removed by gentle washing, and adherent cells were supplemented with complete medium containing 100ng/ml CCL19 (DENOVO). Culture slides were maintained at 37^{o}C in 5% CO_2 on a heated microscope stage and live cell images were recorded at a time-lapse interval of 5min. Individual cell trajectories and distances travelled were analysed in ImageJ using the manual tracking plugin and chemotaxis-migration tool (Ibidi). Tracking was restricted to cells that remained visible within the observation field for ≥50% of the total experiment duration.

Real-Time PCR

BMDCs were lysed with TRIzol (Gibco), and RNA was purified using phenol/chloroform extraction. Complementary DNA was reversed transcribed using SuperScript II Reverse transcriptase kit (Invitrogen). The following primers were used for RTqPCR:

Aldh1a2 Forward: CAGAGAGTGGGAGAGTGTTCC

Aldh1a2 Reverse: CACACAGAACCAAGAGAGAAGG

Aldh2 Forward: GACGCCGTCAGCAGGAAAA

Aldh2 Reverse: CGCCAATCGGTACAACAGC

HPRT Forward: TCAGTCAACGGGGGACATAAA

HPRT Reverse: GGGGCTGTACTGCTTAACCAG

Chromatin immunoprecipitation assay

BMDCs were fixed with 1% paraformaldehyde (Sigma-aldrich) at room temperature for 10min with shaking. Glycine (Sigma-aldrich) was used to quench the reaction and cells were washed with ice-cold PBS. Fixed cells were lysed in RIPA for 10min and chromatin was sheared using Biorupter to approximately 200–300 bp. (Diagenode). H3K27me3 (abcam) or IgG (Sigma-alcrich) antibody-bound Dynabeads (Invitrogen) were added to sonicated lysates overnight at 4°C. Dynabeads were washed with ice-cold RIPA, LiCl buffer and TE before DNA elution. Reverse crosslinking was performed at 65°C for 4h prior to RNaseA (Roche) and Proteinase K treatment (Sigma-aldrich). Ethanol precipitation was performed to further purify DNA fragments before ChIP assay. The following primers were used for ChIP:

Aldh1a2-1 Forward: AAAGCTCTTTCGGGCTGCT,

Aldh1a2-1 Reverse: GCCTTAGCGCTGGTCGG

Aldh1a2-2 Forward: GCTCCGGCCGTCGAG

Aldh1a2-2 Reverse: CGCTTCTTATTGGACGTGCG

Aldh2-1 Forward: AGACTGGGTAGGATGGGACC

Aldh2-1 Reverse: CGTGACTTTGAGCAACCTGC

Aldh2-2 Forward: CTGTGTATGAGCATCGCCCT

Aldh2-2 Reverse : CGGAGTCCGGAACAACTTCA

Hoxa11 Forward: GCTGCGAAGAAGGTGCTGAACG

Hoxa11 Reverse: CGGTGGGTGAGGGATACTCTCTGG

Image acquisition and analysis

Images were visualized at 10x, 20x or 63x magnification using Zeiss LSM 510 Meta or LSM 710 Confocal Microscopes. DAPI staining was used to assess the quality and intactness of different fields of the epidermal sheets and whole mount ear tissues prior to acquisition of LCs/ DCs staining. Z-stacks were acquired for the epidermal sheets and whole mount ear tissues for projection at maximal intensity. All image analyses were performed on LSM Image Browser, Zen 2009 or ImageJ software.

Data and Software Availability

The accession number for the RNA-sequencing data reported in this paper is GEO: GSE122206.

Statistics

Data were analysed by two-tailed Student's *t* test or 2-way ANOVA. P-values <0.05 were considered significant.

Study approval

All mouse protocols were conducted in accordance with the guidelines of the Nanyang Technological University Institutional Animal Care and Use Committee. All experiments with human samples were conducted in accordance with the ethical principles of the Declaration of Helsinki and the protocol was approved by the Institutional Review Board (IRB) of Nagoya City University Graduate School of Medical Sciences. Normal skin specimens from mastectomies were used after informed consent.

Supplemental References

Gunawan, M., Venkatesan, N., Loh, J.T., Wong, J.F., Berger, H., Neo, W.H., Li, L.Y., La Win, M.K., Yau, Y.H., Guo, T.*, et al.* (2015). The methyltransferase Ezh2 controls cell adhesion and migration through direct methylation of the extranuclear regulatory protein talin. Nature immunology *16*, 505-516.